Discovery of Oxygen Carriers by Mining a First-Principle Database

THE JOURNAL OF PHYSICAL CHEMISTRY C
A JOURNAL OF THE AMERICAN CHEMICAL SOCIETY

pubs.acs.org/JPCC

Article

Discovery of Oxygen Carriers by Mining a First-Principle Database

Joakim Brorsson, Viktor Rehnberg, Adam A. Arvidsson, Henrik Leion, Tobias Mattisson, and Anders Hellman*

Cite This: *J. Phys. Chem. C* 2023, 127, 9437−9451

Read Online

ACCESS | Metrics & More | Article Recommendations | Supporting Information

ABSTRACT: Chemical looping is an innovative technique that relies, to a large extent, on the possibility of finding new oxygen carriers. Until now, these materials have primarily been identified via experimental techniques and therefrom derived insights. However, this is both costly and time-consuming. To speed-up this process, we have applied a computational screening approach based on energetic data retrieved from the Open Quantum Materials Database. In particular, we have considered combinations of all mono-, bi-, and trimetallic alloys and mixed oxides with up to three distinctive phases. Here, we specifically focus on a technique referred to as chemical looping oxygen uncoupling, which is especially suitable for solid fuels, e.g., combustion of biomass for negative CO_2 emissions. The formation energies obtained for the materials of interest were used to identify phase transitions that are likely to occur under conditions relevant for chemical looping oxygen uncoupling. Given these criteria, the initial list of 300000 materials is reduced by a factor of 20, and after filtering out rare, radioactive, toxic, or harmful elements only 1000 remain. When considering the abundance of elements in the ranking criteria, most of the highest ranking phases include Cu, Mn, and Fe. This adds credibility to the procedure, as many viable oxygen carriers for chemical looping oxygen uncoupling that have been studied experimentally contain these elements. While Cr-based materials have not been widely explored for this application, our study suggests that this might be worthwhile since these occur more frequently than Fe. Other elements that would be interesting as additional components include Ba, K, Na, Al, and Si.

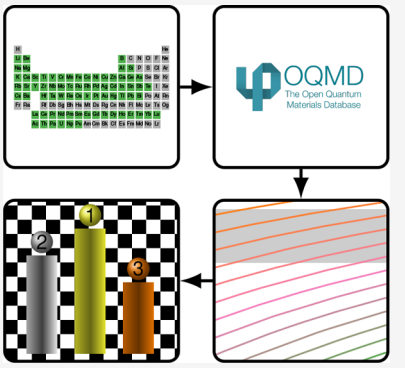

INTRODUCTION

Chemical looping combustion (CLC) represents an emerging technology that can be used for realizing carbon capture and storage (CCS), a key technology for reducing the anthropogenic greenhouse gas emissions and thereby mitigating the effects of global warming.[1−5] This is achieved by transforming the combustion into a two-step process through the cycling of a solid oxygen carrier (OC), often in the form of metal oxide, which is first oxidized in an air chamber and then reduced, in a separate fuel chamber, as the oxygen is partially transferred to the fuel. Consequently, the exhaust gas is, in principle, made up only of H_2O and CO_2. Since these can be easily separated by condensing the former, the CLC process produces a pure CO_2 stream that can be captured. It is also crucial to note that chemical looping has a much broader usage than just combustion, i.e., heat and power generation. In particular, recent research efforts have shown that this technique can be relevant for producing various chemicals, including hydrogen.[2,5,6]

While there exist several different variants of CLC, this study has exclusively focused on chemical looping oxygen uncoupling (CLOU), which distinguishing feature is that the metal oxide spontaneously decomposes, thereby releasing oxygen to the gas phase, under the high temperature and reducing conditions in the fuel reactor.[2−4,7] As a result, there are no direct interactions between the OC and the fuel. The combustion rate of solid hydrocarbons, such as coal and biomass, is therefore not limited by the relatively slow gasification of the char content.[2,8,9] Indeed, it has been demonstrated that this process is 50 times higher when using CLOU, compared to conventional CLC.[10] This makes it well suited for bioenergy with carbon capture and storage (BECCS), which is a key technology for achieving negative carbon emissions,[11,12] and thereby limit global warming to an increase in temperature of, at most, 2 °C by the end of this century.[13]

It should be stressed that large scale (1.5 kW) testing of the CLOU concept has demonstrated that it is possible to simultaneously achieve a high char conversion rate (33% s^{-1}) and carbon capture efficiency (99.3%).[14] More importantly, efficiencies as high as 93% have recently been reported for the combustion of biomass using a similar setup.[15] Simulations moreover indicate that the utilization of CCS based on CLOU in a combined heat and power plant leads to a loss of a mere 1% in net efficiency while allowing the capture of as much as 99.0% (504 kg $MW^{-1}h$) of the emitted CO_2.[16] In fact, Lyngfelt

Received: December 6, 2022
Revised: March 30, 2023
Published: May 14, 2023

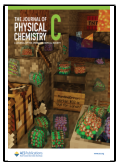

and Leckner[17] have estimated a carbon capture cost of around 20 €$t_{CO_2}^{-1}$ using ilmenite and natural manganese ores. Even for synthetic OCs, which are more expensive, CLC and CLOU should still be considerably cheaper than postcombustion systems for capturing CO_2.

A key issue related to the development of CLC is the identification of suitable OCs, since the latter must generally satisfy a variety of different criteria.[2−5,18] This includes favorable thermodynamics and kinetics, with respect to oxidation and reduction, as well as a significant oxygen storage capacity. Various practical aspects such as high chemical and mechanical stability to prevent breakage, agglomeration, attrition, and fouling together with low cost, toxicity, and environmental impact are, however, equally important. Since it is challenging to enhance the efficiency of existing OCs, there is a strong need for finding new materials.[5,19] Fortunately, high-throughput screening that utilizes the efficiency of modern computers and the ever-increasing volume of data stored in publicly available databases provides a viable route for achieving this goal.

A practical benefit with the CLOU process is that the fuel need not be taken into account when assessing the potential of a prospective OC; it is enough to consider the transformation between the oxidized and reduced phase. It has therefore been possible to identify candidate materials based solely on thermodynamic principles by searching the first-principles data found in the Open Quantum Materials Database (OQMD).[20,21] In what follows, we first describe the methodology, beginning with the thermodynamic relationships used to determine the theoretical viability, followed by the procedure for generating and ranking the possible candidates. Next, we present the main results of the study by first showing overall statistics and then listing the highest-ranking transitions before providing a detailed analysis of the interactions between some of the most frequently occurring metals. This is followed by an in-depth discussion of the phases that appear among the top 20 candidates. Finally, we summarize our major conclusions and give our view on how these can contribute to future studies.

METHODS

Density functional theory (DFT) represents a widespread computational method that can provide information regarding the properties of solid state materials, including many that are of interest when assessing the suitability of a given metal oxide as an OC. Nevertheless, such calculations can be quite demanding, which limits the number of compounds that can be assessed in a given study. Fortunately, there are multiple publicly available databases containing information obtained via such calculations for a wide variety of different materials. Notable examples include the OQMD,[20,21] which has been used in this study, the Materials Project database,[22] the aflowlib.org library[23,24] as well as the Novel Materials Discovery (NOMAD) Laboratory.[25] At the time of writing, the OQMD contains information for a total of 1022603 different materials, which includes both structural and thermodynamic properties.[26] These have more precisely been obtained via DFT calculations using the implementation of the projector augmented wave (PAW)[27,28] in the Vienna ab initio simulation package (VASP),[29] based on potentials in which exchange-correlation effects have been treated as described by Perdew−Burke−Ernzerhof (PBE).[30] It has also been ensured that the crystal structures and electronic ground states have been converged within 0.001 eV atom^{-1} and 0.0001 eV atom^{-1}, respectively.[26] Moreover, the calculation parameters have been rigorously tested[20,21] so as to give a mean absolute error of 0.096 eV atom^{-1} for the estimated formation energies compared with reported measurements for 1670 materials. This includes optimizing the U values, which are crucial to obtaining good agreement for, among others, metal oxides. Corrections have moreover been introduced to compensate for certain shortcomings inherent to DFT calculations, e.g., the incompatibility of results obtained with the generalized gradient approximation (GGA) and GGA+U methods, respectively.

The first step of the procedure is to retrieve the formation energies for all mono-, bi-, and trimetallic oxides, as well as the corresponding reduced phases. Next, combinatorics is used to generate a complete subspace that contains all available compounds and mixtures thereof with a fixed ratio between the metallic elements (see Supplementary Note S1). Note that in the monometallic case, a single material consists of all compounds Me_xO_y. After that, the given candidate's potential to act as an OC for CLOU is quantified in terms of key thermodynamic properties. To help identify the most promising material systems for practical applications, we have ranked the candidates based on the average abundance of the constituent elements (in the earth's crust) and, in addition, provide estimates of the oxygen transfer capacity (OTC).

Thermodynamic Criteria. To be suitable for CLOU, a metal oxide must undergo a phase transition at a relevant temperature and partial O_2 pressure.[31] An additional requirement is that it should provide a sufficient O_2 transport to the gas phase in order to oxidize the fuel via normal combustion. Still, the reduced OC also needs to be reoxidized in the air reactor at a sufficiently low oxygen pressure, so as not to decrease the efficiency of the power process by any significant extent. This means that one must, in principle, include both thermodynamic and kinetic aspects when judging the performance of candidate materials. While there exists a few such studies[32,33] based on first-principles calculations, these have been limited to one or a few different materials and the techniques used therein would not be practical in a high-throughput study such as the one at hand. Furthermore, the understanding of the coupling between the structure and performance of OCs for CLOU is still relatively poor,[34] making it difficult to identify physical descriptors. For this reason, the selection has been performed based purely on thermodynamical arguments.

While it is customary to use $p_{O_2} \lesssim 5$ kPa,[31,35] we have employed a much wider range, specifically 10^{-6} MPa $\leq p_{O_2} \leq 1$ MPa. This is mainly to ensure that we do not miss possible candidates. Nevertheless, the chosen values on the upper and lower bounds also reflect the uncertainty in the calculations (see Supplementary Note S2, Table S1, and Figure S1). Moreover, the utilization of oxygen carriers with an equilibrium oxygen pressure higher or lower than 5 kPa may be feasible in other chemical looping processes.[36] The operating temperature, meanwhile, normally falls between 900 and 1000 °C in the air reactor, since many good OCs release oxygen within this range,[34] and the temperature in the fuel reactor is typically somewhat lower. One should note, however, that there are significant variations in the reported conditions. Here, we have chosen to consider a broader interval, namely 750 °C−1050 °C, based on similar arguments

https://doi.org/10.1021/acs.jpcc.2c08545
J. Phys. Chem. C 2023, 127, 9437−9451

as for the O_2 pressure. Though the use of such broad ranges for the critical parameters clearly has both advantages and disadvantages, it is deemed relevant since the purpose of the study at hand is to (i) illustrate a new type of methodology and (ii) identify potential candidates that may be worthwhile to investigate in the future.

To check if a given material complies with the above conditions, it is necessary to find the most stable phases at any given chemical potential, which represents a so-called convex hull.[37] To do so, we have followed a previously reported procedure for constructing open phase diagrams.[19,38−40] From a thermodynamic perspective, this means considering the OC as an isothermal and isobaric system closed for all species except oxygen, which can therefore be described by a grand canonical potential of the form

$$\begin{aligned}\phi(T, P, N_{\mathrm{Me}_1}, ..., N_{\mathrm{Me}_n}, \mu_{\mathrm{O2}}) &= G(T, P, N_{\mathrm{Me}_1}, ..., N_{\mathrm{Me}_n}, \mu_{\mathrm{O2}}) \\ &\quad - \mu_{\mathrm{O}_2} N_{\mathrm{O}_2}(T, P, N_{\mathrm{Me}_1}, ..., N_{\mathrm{Me}_n}, \mu_{\mathrm{O2}}) \\ &= E(T, P, N_{\mathrm{Me}_1}, ..., N_{\mathrm{Me}_n}, \mu_{\mathrm{O2}}) \\ &\quad + PV(T, P, N_{\mathrm{Me}_1}, ..., N_{\mathrm{Me}_n}, \mu_{\mathrm{O2}}) \\ &\quad - TS(T, P, N_{\mathrm{Me}_1}, ..., N_{\mathrm{Me}_n}, \mu_{\mathrm{O}_2}) \\ &\quad - \mu_{\mathrm{O}_2} N_{\mathrm{O}_2}(T, P, N_{\mathrm{Me}_1}, ..., N_{\mathrm{Me}_n}, \mu_{\mathrm{O}_2}) \end{aligned} \quad (1)$$

Here, G, E, S, and V represent the Gibbs free energy, internal energy, entropy, and volume of the system, respectively, while $\{\mathrm{Me}_i\}_{i=1}^{n}$ are the n metallic elements. This expression can be simplified by recognizing the fact that the volume difference between the solid phases is generally quite small. In addition, the entropy is dominated by the contribution from the O_2 gas, which is contained within the chemical potential μ_{O_2}. It should be emphasized that the same approximations have been used in earlier studies.[19,38−40] Specifically, considering the entropy of the solid phases requires, at the very least, harmonic phonon calculations, which are too demanding when screening several hundred thousand compounds.

After omitting the PV and TS terms and normalizing with respect to the total number of metal atoms,

$$N_{\mathrm{Me}} = \sum_{i=1}^{n} N_{\mathrm{Me}_i} \quad (2)$$

eq 1 takes on the form

$$\bar{\phi} = \frac{\phi}{N_{\mathrm{Me}}} \approx \frac{E - \mu_{\mathrm{O}_2} N_{\mathrm{O}_2}}{N_{\mathrm{Me}}} \quad (3)$$

where we have dropped the functional dependence for the sake of brevity. The potential for the most stable phase combinations can, hence, be represented by a collection of straight line segments with intercepts E/N_{Me} and slopes $-N_{\mathrm{O}_2}/N_{\mathrm{Me}}$. Together these will form a convex hull in the $\bar{\phi}$−μ_{O_2} space (see Figure 1a and Figure S2). The transformations occur as the environment changes from being reducing to oxidizing and thus correspond to the intersections between the lines that, for a specific chemical potential, gives the lowest $\bar{\phi}$. If one considers Cu_xO_y, for instance, metallic Cu is the most stable for oxygen potentials up to ∼ −4 eV O_2^{-1}. At this point, the corresponding horizontal line is intersected by Cu_2O, which has a slope of −0.5. CuO, for the which the inclination is even higher (slope −1), has the lowest energy above ∼ −2 eV O_2^{-1}, however.

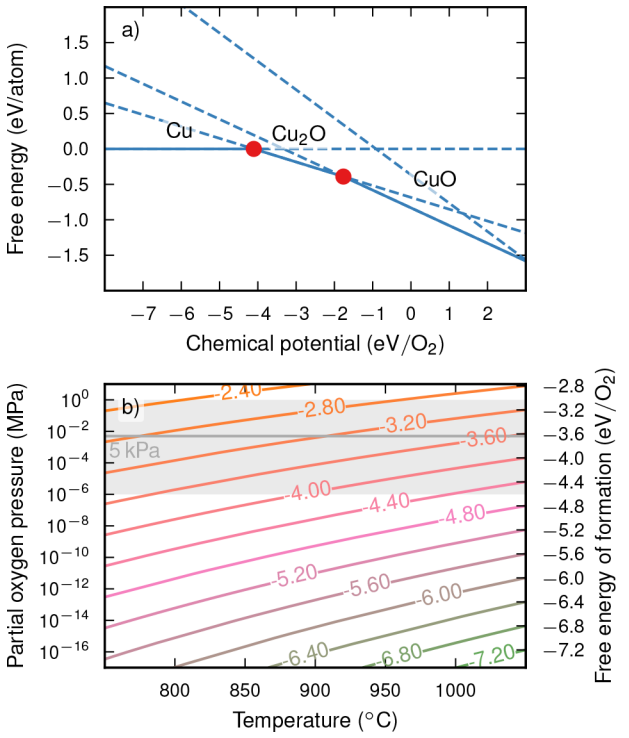

Figure 1. (a) Free energy of formation as a function of the oxygen chemical potential for metallic copper and copper oxides (dashed blue lines) in which the most stable phase at a given chemical potential (solid blue lines) as well as the transformations between them (red dots) have been highlighted. (b) Modified Ellingham diagram displaying the partial oxygen pressure as a function of the temperature, where each line represents a hypothetical phase transition with a specific value for the free energy of the reaction.

It is possible to construct a so-called Ellingham diagram (see Figure 1b) by considering the transition between a pair of phases (red circles in Figure 1a). To do so, we use the fact that the oxygen chemical potential can be expressed as a function of the temperature and pressure,[5]

$$\mu_{\mathrm{O}_2}(T, p) = \mu^0_{\mathrm{O}_2}(T, p^0) + \frac{1}{2} \ln\left(\frac{p}{p^0}\right) \quad (4)$$

Here $\mu^0_{\mathrm{O}_2}(T, p^0)$ corresponds to tabulated reference values at 1 atm.[41,42] This enables us to select candidates based on the requirement that the curve must cross the area that corresponds to a pressure 10^{-6} MPa ≤ p_{O_2} ≤ 1 MPa and temperature 750 °C ≤ T ≤ 1050 °C. While Ellingham diagrams are conventionally used to represent the oxidation of individual phases,[36] we apply it in a broader context. More precisely, we include lines that correspond to reactions between combinations of mixed metal oxides and alloys that involve the release of oxygen gas.

Additional Properties. The OTC[3] is perhaps the most crucial property for any OC since it correlates to the amount of oxygen that can be provided to the fuel chamber. It is, therefore, related to the rate at which solids must be transferred between the air and fuel reactors to achieve full combustion. Nevertheless, experiments have shown that the theoretical OTC is rarely reached, as the recirculation also

https://doi.org/10.1021/acs.jpcc.2c08545
J. Phys. Chem. C 2023, 127, 9437−9451

Table 1. Summary of the Screening Process Aimed at Identifying Potential Candidates for CLOU among Oxides Made up of One ($n \leq 1$), Two ($n \leq 2$), or Three Metallic Elements ($n \leq 3$), with and without Filtering

Species	Elements considered	Combinations	Convex hulls	OC materials	Stable transitions	Candidate transitions
$n = 1$ (unfiltered)	101	101	73	20	169	22
$n = 1$ (filtered)	26	26	26	8	74	8
$n = 2$ (unfiltered)	101	5151	21836	783	125348	923
$n = 2$ (filtered)	26	351	3346	152	21679	180
$n = 3$ (unfiltered)	101	171801	303919	14030	2550698	17116
$n = 3$ (filtered)	26	2951	16295	1010	142973	1278

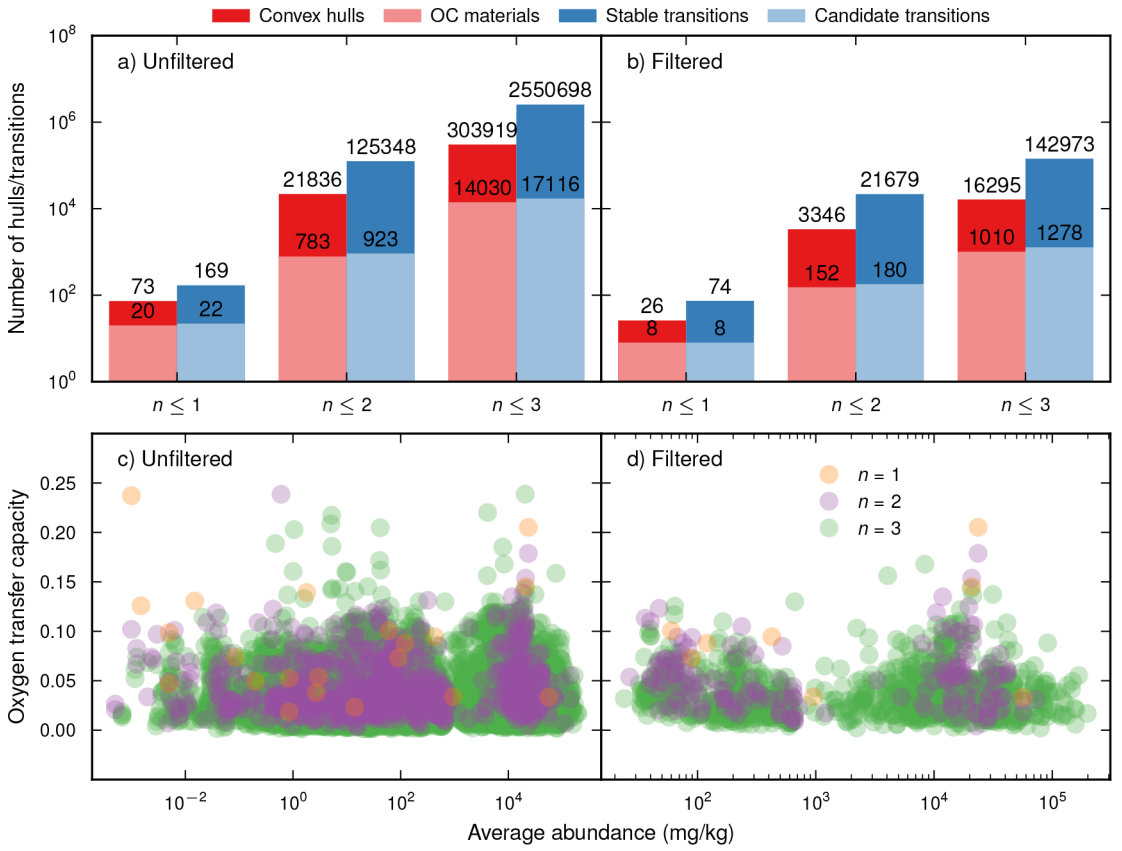

Figure 2. Diagrams summarizing the results obtained with (a, c) and without (b, d) filtering. This includes (a, b) the number of convex hulls (dark red) and potential OCs (light red) together with the number of stable (dark blue) and candidate (light blue) transitions for systems, with up to one ($n \leq 1$), two ($n \leq 2$), and three ($n \leq 3$) metallic elements. The (c, d) the oxygen transfer capacity as a function of the average abundance is also shown, which includes data for all mono-, bi-, and trimetallic materials represented by the orange, purple, and green circles, respectively.

needs to be sufficiently high to fulfill the heat balance. To estimate the upper limit, we will assume that the amount of fuel combusted relative to the mass of the OC is equivalent to the amount of oxygen released in the phase transition of the OC. In the monometallic case, the oxidation can be represented by the reaction

$$a\mathrm{Me}_x\mathrm{O}_y + \mathrm{O}_2 \rightleftharpoons a\mathrm{Me}_x\mathrm{O}_{y+2/a} \tag{5}$$

and the transfer capacity can be written as

$$\mathrm{OTC} = \frac{m_{\mathrm{O}_2}}{a m_{\mathrm{Me}_x\mathrm{O}_{(y+2/a)}}} = \frac{m_{\mathrm{Me}_x\mathrm{O}_{(y+2/a)}} - m_{\mathrm{Me}_x\mathrm{O}_y}}{m_{\mathrm{Me}_x\mathrm{O}_{(y+2/a)}}} \tag{6}$$

where m_i is the mass of the compound i.

Since multiple factors determine the practical usability of an OC, we have considered both a filtered and an unfiltered list of materials. In the former case, we have, more precisely, omitted elements that are either radioactive, toxic, environmental hazards, or harmful to people.[43] It should be stressed, however, that no consideration has been taken with respect to melting temperature and volatility since these are difficult to assess based on first-principle calculations alone. They can neither be readily estimated for oxide phases based solely on the constituent elements. One should, therefore, keep in mind that some of the candidates identified in this study might not be solid, or even stable, at the temperatures of interest. Though this could, moreover, rule out certain alkali components, these have been used with OCs in order to increase activity despite being known precursors for corrosion during biomass combustion.[36,44,45] Note also that similar arguments apply to, for instance, the mechanical strength or rate of oxidation and reduction.

Since the market prices of individual elements depend on many physical, economic, and political factors, these should be expected to vary substantially over time. For this reason, it is

https://doi.org/10.1021/acs.jpcc.2c08545
J. Phys. Chem. C 2023, 127, 9437−9451

deemed more suitable to compare the average abundance of the constituent metallic elements in the crust of the earth,[46]

$$\overline{X} = \frac{\sum_{\mathrm{Me}} n_{\mathrm{Me}} X_{\mathrm{Me}}}{\sum_{\mathrm{Me}} n_{\mathrm{Me}}} \quad (7)$$

where X_{Me} is the abundance of the element Me and n_{Me} the number of such atoms in the compound. Because of its significance, this property has been given a dual purpose. First, we have excluded all metals (Me) with an abundance $X_{\mathrm{Me}} < 1.0$ mg kg^{-1} from the filtered list. In addition, $\overline{X}$ is used for ranking the potential candidates.

RESULTS AND DISCUSSION

The procedure presented in the previous section has been applied to three distinct subsets, namely mono-, bi-, and trimetallic materials. Specifically, this has involved ranking all transitions that could be constructed from mixtures of compounds extracted from the OQMD. In what follows, we will first discuss some overall statistics related to this process. We then take a careful look at the final list of candidates before considering the interactions between the most frequently occurring metals with a number of common ash elements. Finally, we present some additional information from the literature about the phases that appear among the top 20 candidates to showcase both the potential and limits of the results obtained in this study.

Overall Statistics. Starting with 100 metallic elements, we found a total of 73 (169), 21836 (125348), and 303919 (2550698) unfiltered materials (stable transitions) consisting of up to one, two, and three different metals respectively (see Table 1 and Figure 2). It should be noted that each is represented by a convex hull that encompasses the most stable combinations of oxides and alloys with a given ratio between the metallic elements. In the monometallic case this would correspond to all compounds of the form Me_xO_y. Specifically, we identify a given material as a potential OC if any of the associated phase transitions occur under CLOU conditions. From this analysis, we find that 20 (22), 783 (923), and 14030 (17116) of the hulls (transitions) satisfy our criteria. Although this corresponds to a vast number of candidates, we have achieved a considerable reduction in the number of data points. When instead considering the data obtained for the 26 elements (see Figure S3) that remain after filtering out those that are identified as toxic, radioactive, hazardous, harmful to the environment, or too rare, the corresponding lists become significantly shorter. More precisely, only 8 (8), 152 (180), and 1010 (1278) of the mono-, bi-, and trimetallic hulls (transitions), out of 26 (74), 3346 (21679) and 16295 (142973), respectively, are viewed as promising OCs for CLOU.

As is evident from the overall analysis presented above, the number of potential materials among the monometallic systems is quite limited. While the estimated OTC seems to be almost independent of the number of elements, it tends to be smaller, although only marginally, for compounds with a lower average abundance. This is not unexpected, however, since heavier elements are usually less abundant and the transitions involving many such atoms will release less oxygen per mass unit. Since the atomic number is correlated with the mass, toxicity, radioactivity, and abundance the OTC actually reflects several practically relevant factors. The fact that the OTC is somewhat larger for lighter elements should thus be regarded as positive. As expected, the number of candidate transitions increases dramatically if the transitions are allowed to involve more elements (see Figure 3). Additional atomic

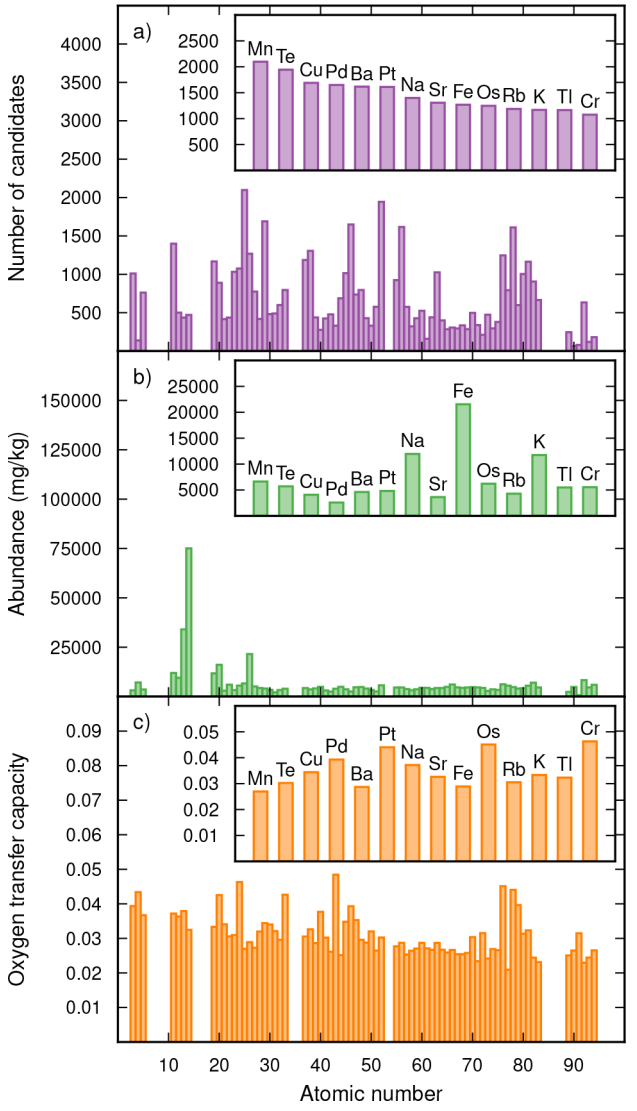

Figure 3. Number of candidates (a) together with the abundance (b) and oxygen transfer capacity (c) versus the atomic number. Note that the two latter properties have been calculated as averages over all transitions that involve a given element. The corresponding insets show the same data for the 14 most frequently appearing metals.

species can also induce other benefits, such as increased stability against sintering or attrition. Though it is not possible to identify any clear trends with respect to the number of candidates, it should be noted that this result could be influenced by the availability of source data. Still, an overall analysis indicates that most elements are found in a similar number of entries in the OQMD (see Figure S5). While there exists a few outliers, it is worth mentioning that the frequent occurrence of boron and yttrium, in this database, is not reflected in the list of candidates (see Figure 4).

Ranking of Transitions. Even though the individual transitions have been ranked based on the average abundance several of the highest ranking OCs (see Table 2) contain chemical species that would make them unsuitable for real-life applications. For this reason, we will henceforth focus on the

https://doi.org/10.1021/acs.jpcc.2c08545
J. Phys. Chem. C 2023, 127, 9437−9451

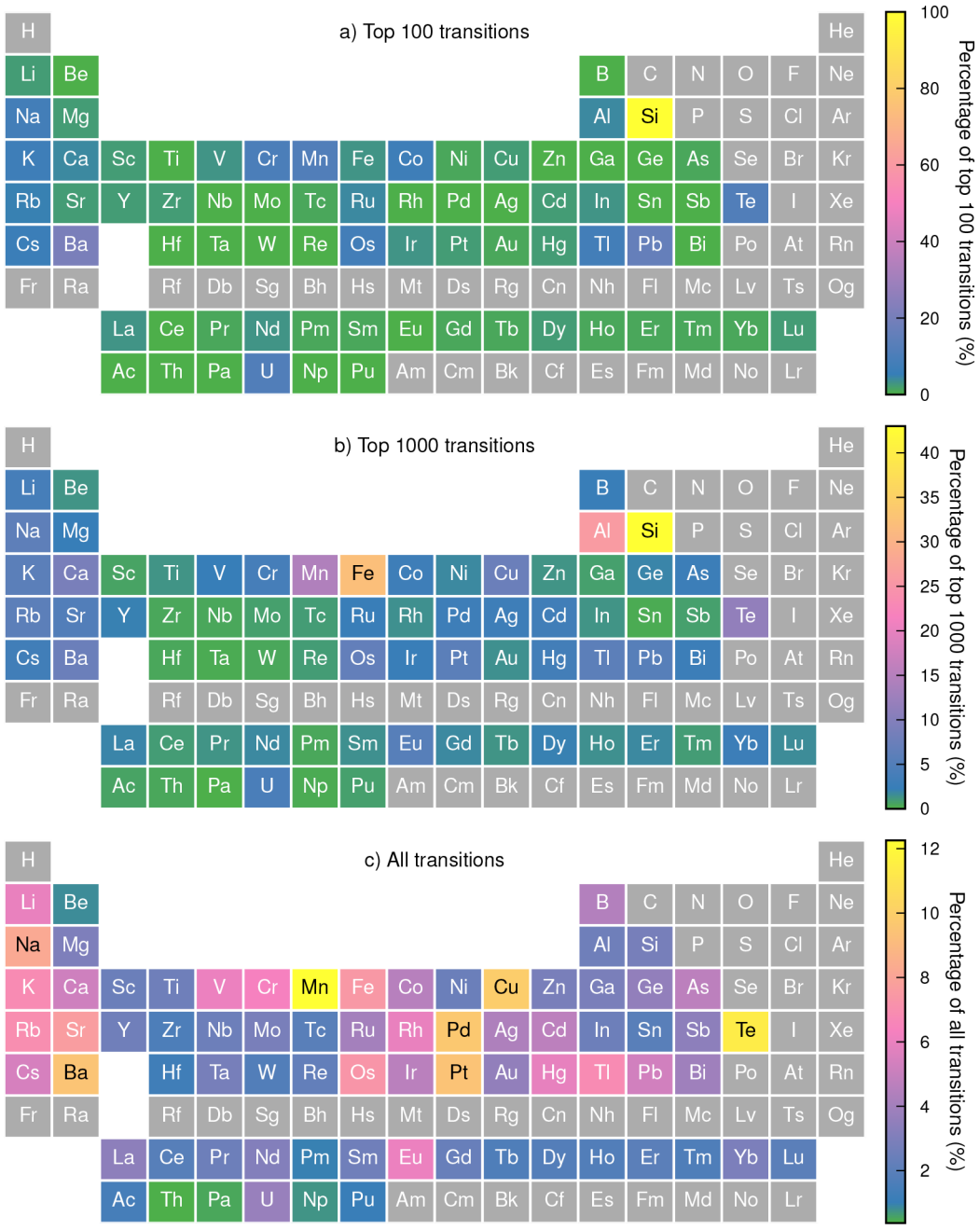

Figure 4. Periodic tables where the percentage among the top 100 (a) and 1000 (b) candidates as well as the entire list (c) that contain a given metallic element has been indicated.

list obtained after filtering out elements that are either radioactive, toxic, harmful to people, environmental hazards, or rare. Although this reduces the number of entries considerably, namely from 17116 to 1278 when considering all materials with up to three distinct metals, it is practically unfeasible to discuss all of them in detail. As an example of how to utilize these results, we will therefore focus on the top 20 filtered candidates and only present statistical measures based on all of the transitions.

Before proceeding with the analysis, it is important to note that the occurrence of a given metallic element among the top 100 candidate will mainly be determined by the average abundance. By instead including the entire list, one obtains a measure of the extent by which a given metal confers CLOU properties based on the thermodynamic criteria. To check the conclusions drawn by analyzing these two lists, we have also considered the first 1000 entries (see Figure 4) because this will, to some extent, capture both trends.

Silicone dominates the top of the leaderboard (see Figure 5 and Figure 4 as well as Table 2) and is found in 68.0% (100.0 percent) of the top 100 (un) filtered candidates. Still, the occurrence in the entire list is just 7.0% (2.8%). This clearly indicates that oxides containing Si, though interesting from an economic perspective, might not have the highest probability of being suitable OCs. Manganese, meanwhile, is involved in as many as 35.0% (12.3%) of all (un) filtered candidates and should, according to the same logic, be the most likely to provide CLOU capabilities. At the same time, it has a relatively high abundance and, hence, appears in 35.0% (11.0%) of the 100 highest-ranking transitions. This is a key result, since there

https://doi.org/10.1021/acs.jpcc.2c08545
J. Phys. Chem. C 2023, 127, 9437−9451

Table 2. List of the 20 Highest Ranking Candidates for CLOU among the Filtered Transitions

Place	Transition	Oxygen transfer capacity	Average Abundance
1st	$4BaFeSi_4O_{10} + O_2 \rightleftharpoons 2Fe_2O_3 + 8SiO_2 + 4BaSi_2O_5$	0.0169	1.97×10^5
2nd	$\frac{2}{3}Cr_2O_3 + \frac{4}{3}K_2Si_4O9 + O_2 \rightleftharpoons \frac{16}{3}SiO_2 + \frac{4}{3}K_2CrO_4$	0.0552	1.67×10^5
3rd	$\frac{7}{3}Mn_2Al_4Si_5O_{18} + O_2 \rightleftharpoons \frac{19}{3}SiO_2 + \frac{14}{3}Al_2SiO_5 + \frac{2}{3}Mn_7SiO_{12}$	0.0208	1.58×10^5
4th	$\frac{32}{3}BaSi_2O_5 + \frac{14}{3}Ba_2MnSi_2O_7 + O_2 \rightleftharpoons 10Ba_2Si_3O_8 + \frac{2}{3}Mn_7SiO_{12}$	0.00607	1.57×10^5
5th	$\frac{2}{3}Cr_2O_3 + \frac{8}{3}Ba_2Si_3O_8 + O_2 \rightleftharpoons \frac{4}{3}BaCrO_4 + 4BaSi_2O_5$	0.0223	1.54×10^5
6th	$\frac{2}{3}Cr_2O_3 + \frac{4}{9}Rb_6Si_{10}O_{23} + O_2 \rightleftharpoons \frac{40}{9}SiO_2 + \frac{4}{3}Rb_2CrO_4$	0.0493	1.48×10^5
7th	$\frac{7}{6}CaMn_4Si_5O_{15} + O_2 \rightleftharpoons 4SiO_2 + \frac{7}{6}CaSiO_3 + \frac{2}{3}Mn_7SiO_{12}$	0.0411	1.46×10^5
8th	$\frac{2}{3}Cr_2O_3 + \frac{8}{3}K_2Si_2O_5 + O_2 \rightleftharpoons \frac{4}{3}K_2CrO_4 + \frac{4}{3}K_2Si_4O_9$	0.0454	1.35×10^5
9th	$\frac{19}{3}Al_2O_3 + \frac{7}{3}Mn_2Al_4Si_5O_{18} + O_2 \rightleftharpoons 11Al_2SiO_5 + \frac{2}{3}Mn_7SiO_{12}$	0.0146	1.33×10^5
10th	$\frac{2}{3}Cr_2O_3 + \frac{10}{3}Rb_2Si_2O_5 + O_2 \rightleftharpoons \frac{4}{3}Rb_2CrO_4 + \frac{2}{3}Rb_6Si_{10}O_{23}$	0.0277	1.28×10^5
11th	$4Ba_2FeSi_2O_7 + O_2 \rightleftharpoons 2Fe_2O_3 + 8BaSiO_3$	0.0158	1.24×10^5
12th	$\frac{2}{3}Cr_2O_3 + 4BaSiO_3 + O_2 \rightleftharpoons \frac{4}{3}BaCrO_4 + \frac{4}{3}Ba_2Si_3O_8$	0.0324	1.21×10^5
13th	$Ba_2SiO_4 + 4Ba_2FeSi_2O_7 + O_2 \rightleftharpoons BaFe_4O_7 + 9BaSiO_3$	0.0134	1.2×10^5
14th	$4Ba_2MnSi_2O_7 + O_2 \rightleftharpoons 2Mn_2O_3 + 8BaSiO_3$	0.0158	1.13×10^5
15th	$2Cr_2O_3 + \frac{8}{3}Na_2Si_2O_5 + O_2 \rightleftharpoons \frac{4}{3}Na_2CrO_4 + \frac{8}{3}NaCrSi_2O_6$	0.0389	1.11×10^5
16th	$2Ba_2SiO_4 + 2Ba_2MnSi_2O_7 + O_2 \rightleftharpoons 2BaMnO_3 + 6BaSiO_3$	0.0182	1.06×10^5
17th	$\frac{14}{3}MgMnSiO_4 + O_2 \rightleftharpoons \frac{5}{3}SiO_2 + \frac{7}{3}Mg_2SiO_4 + \frac{2}{3}Mn_7SiO_{12}$	0.0385	1.02×10^5
18th	$\frac{17}{6}Ca_2SiO_4 + \frac{1}{2}Mn_7SiO_{12} + O_2 \rightleftharpoons \frac{7}{6}Ca_2Mn_3O_8 + \frac{10}{3}CaSiO_3$	0.0389	9.43×10^4
19th	$4VO_2 + 2Sc_2Si_2O_7 + O_2 \rightleftharpoons 4SiO_2 + 4ScVO_4$	0.0364	9.4×10^4
20th	$4K_4CuSi_2O_7 + O_2 \rightleftharpoons 4KCuO_2 + 4K_2SiO_3 + 2K_2Si_2O_5$	0.0202	9.25×10^4

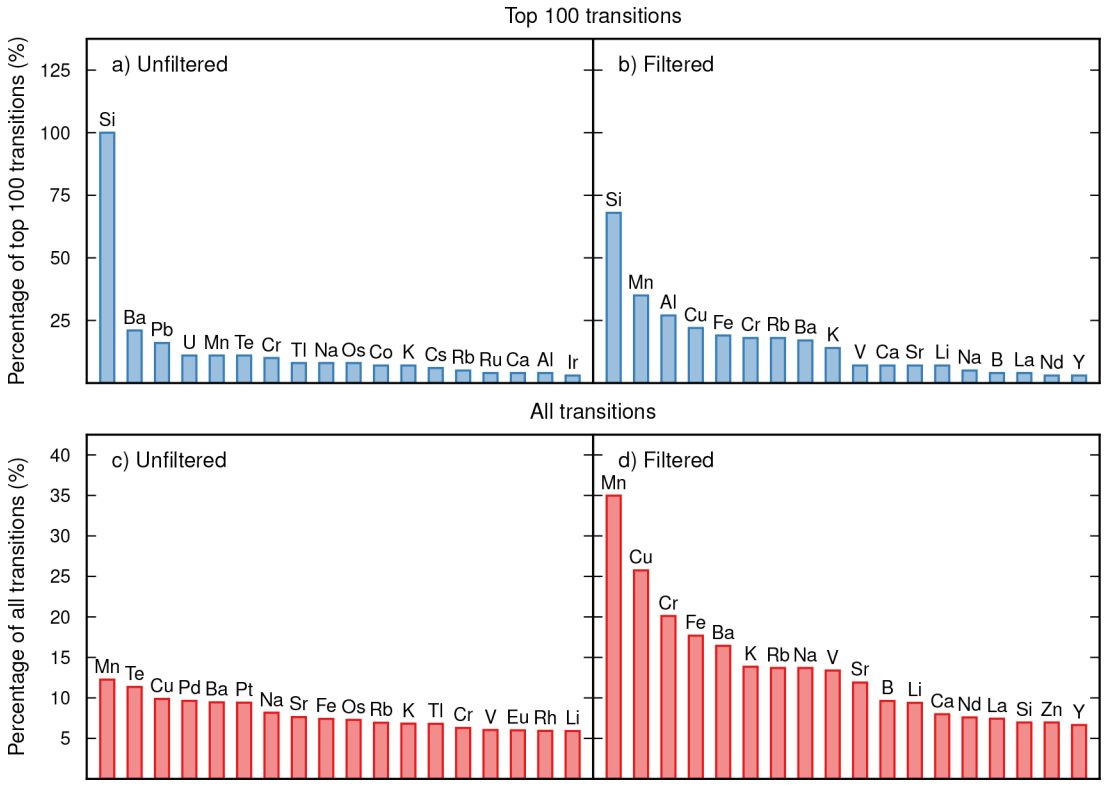

Figure 5. Percentages among (a, b) the top 100 and (c, d) the entire list of unfiltered (a, c) and filtered (b, d) transitions that contain a given metallic element.

is strong experimental evidence that Mn-based oxides display CLOU properties.[2,34] The same holds true for Cu, which occurs in 25.7% (9.9%) of the entries and is the second (third) most common element in the (un) filtered list. Interestingly Cr is the third and Fe the fourth most frequently appearing metal among the filtered transitions. This is somewhat surprising

https://doi.org/10.1021/acs.jpcc.2c08545
J. Phys. Chem. C 2023, 127, 9437−9451

Table 3. List of the 20 Highest Ranking Candidates for CLOU among the Filtered Transitions That Do Not Contain Si

Place	Transition	Oxygen transfer capacity	Average Abundance
58th	$4Fe_3O_4 + O_2 \rightleftharpoons 6Fe_2O_3$	0.0334	5.63×10^4
60th	$6MnAl_2O_4 + O_2 \rightleftharpoons 6Al_2O_3 + 2Mn_3O_4$	0.0299	5.52×10^4
61st	$\frac{2}{3}Cr_2O_3 + \frac{4}{3}BaAl_4O_7 + O_2 \rightleftharpoons \frac{8}{3}Al_2O_3 + \frac{4}{3}BaCrO_4$	0.0525	5.5×10^4
62nd	$\frac{2}{3}Cr_2O_3 + \frac{4}{3}SrAl_4O_7 + O_2 \rightleftharpoons \frac{8}{3}Al_2O_3 + \frac{4}{3}SrCrO_4$	0.0589	5.49×10^4
66th	$\frac{4}{3}LaAlO_3 + \frac{8}{3}MnAl_2O_4 + O_2 \rightleftharpoons \frac{10}{3}Al_2O_3 + \frac{4}{3}LaMn_2O_5$	0.0411	5.17×10^4
68th	$4Fe_2CuO_4 + 4RbFe_{11}O_{17} + O_2 \rightleftharpoons 26Fe_2O_3 + 4RbCuO_2$	0.00656	4.88×10^4
69th	$Mn_2O_3 + 2RbFe_{11}O_{17} + O_2 \rightleftharpoons 11Fe_2O_3 + 2RbMnO_3$	0.015	4.77×10^4
72nd	$\frac{2}{3}Cr_2O_3 + \frac{8}{3}BaAl_2O_4 + O_2 \rightleftharpoons \frac{4}{3}BaAl_4O_7 + \frac{4}{3}BaCrO_4$	0.0393	4.72×10^4
73rd	$\frac{2}{3}Cr_2O_3 + \frac{8}{3}SrAl_2O_4 + O_2 \rightleftharpoons \frac{4}{3}SrAl_4O_7 + \frac{4}{3}SrCrO_4$	0.047	4.71×10^4
74th	$2BaAl_2O_4 + 4AlCuO_2 + O_2 \rightleftharpoons 4CuO + 2BaAl_4O_7$	0.031	4.71×10^4
75th	$4AlCuO_2 + 2SrAl_2O_4 + O_2 \rightleftharpoons 4CuO + 2SrAl_4O_7$	0.0343	4.71×10^4
78th	$22Ca_2Fe_2O_5 + 2CaMn_2O_4 + O_2 \rightleftharpoons 22CaFe_2O_4 + 4Ca_6MnO_8$	0.00497	4.67×10^4
79th	$4Fe_3O_4 + 12NdAlO_3 + O_2 \rightleftharpoons 6Al_2O_3 + 12NdFeO_3$	0.00892	4.62×10^4
80th	$4Fe_3O_4 + 12LaAlO_3 + O_2 \rightleftharpoons 6Al_2O_3 + 12LaFeO_3$	0.00908	4.62×10^4
81st	$4KAlO_2 + Na_7Al_3O_8 + O_2 \rightleftharpoons 4KO + 7NaAlO_2$	0.0403	4.58×10^4
82nd	$4Fe_3O_4 + \frac{12}{11}Rb_2TiO_3 + O_2 \rightleftharpoons \frac{12}{11}RbFe_{11}O_{17} + \frac{6}{11}Rb_2Ti_2O_5$	0.0256	4.47×10^4
83rd	$2Mn_2O_3 + \frac{16}{3}SrAl_2O_4 + O_2 \rightleftharpoons \frac{8}{3}SrAl_4O_7 + \frac{4}{3}Sr_2Mn_3O_8$	0.0222	4.42×10^4
84th	$\frac{2}{3}Cr_2O_3 + \frac{8}{3}NaAlO_2 + O_2 \rightleftharpoons \frac{4}{3}Al_2O_3 + \frac{4}{3}Na_2CrO_4$	0.0909	4.24×10^4
85th	$2Fe_3BO_5 + O_2 \rightleftharpoons 2Fe_3BO_6$	0.0583	4.22×10^4
86th	$\frac{1}{3}Ca_3Al_4O_9 + \frac{2}{3}CaCr_2O_4 + O_2 \rightleftharpoons \frac{1}{3}CaAl_4O_7 + \frac{4}{3}CaCrO_4$	0.109	4.13×10^4

since the former has not been widely explored in this context while the latter is found in many good OCs. It is important to note that Mn, Cu, Cr, and Fe not only appear to confer CLOU properties but are also fairly abundant.

Additional noteworthy elements are Al, Ba, K, Rb, Na, and V. After comparing their relative occurrence, Ba > K $\gtrsim$ Rb $\gtrsim$ Na $\gtrsim$ V > Al, and abundance, Al > Na > K $\gg$ Ba > V > Rb, one can conclude that oxides made up of Na or Ba together with Mn, Cu, Cr, and Fe appear to be the most interesting. In particular, such materials should be reasonably cheap and have a fair chance of being suitable OCs for CLOU. Even though Si or Al are less likely to enhance the CLOU properties, one could consider adding either as an extra component to reduce the cost. In addition, we have found that especially Mn has a comparatively high probability of forming new OCs through interactions with common ash elements (see Figure S6 and Supplementary Note S3). Even though the number of possibilities is lower for Cu, Cr, and Fe as well as Na and Ba, there exists significant variations depending on the composition of the ash. As such, one could potentially match the OC with a specific fuel.

The 20 Highest Ranking Transitions. From a practical perspective, it is especially interesting to consider combinations of compounds that have never been explored as OCs. For convenience, however, we will limit the following discussion to the 20 highest-ranking filtered transitions (see Table 2 and Table 3). As will become apparent, there are several interesting trends and the discussion has, therefore, been divided into a number of subsections concerning candidates with similar composition. In particular, many transitions involve one or more phases that are either identical or chemically similar. In cases where the only difference between a pair of candidates is the identities of the elements, it can be assumed that a new OC suitable for CLOU would be obtained by mixing the two. This is an intriguing prospect, since the resulting enhancement of the entropic contribution to the free energy could help stabilize the stoichiometric phase as well as oxygen vacancies.[47]

Ba−Fe−Si-System. The highest ranking transition, as well as two others, involves barium, iron, and silicone,

$$4BaFeSi_4O_{10} + O_2 \rightleftharpoons 2Fe_2O_3 + 8SiO_2 + 4BaSi_2O_5 \quad (8)$$

$$4Ba_2FeSi_2O_7 + O_2 \rightleftharpoons 2Fe_2O_3 + 8BaSiO_3 \quad (9)$$

$$Ba_2SiO_4 + 4Ba_2FeSi_2O_7 + O_2 \rightleftharpoons BaFe_4O_7 + 9BaSiO_3 \quad (10)$$

This is interesting since such combinations have not been explored in this context, even though iron oxides are well-known oxygen carriers. Unfortunately, the reduced phase $BaFeSi_4O_{10}$ has been found to decompose in air already at 570 °C,[48,49] far below the temperature range of interest for practical applications. This also applies to $BaFe_4O_7$, which breaks down at ∼650 °C.[50] The stability of $Ba_2FeSi_2O_7$, however, is potentially higher since it can be obtained with a 96.5% phase purity via a solid state reaction at 1050 °C.[51,52] Sanbornite ($BaSi_2O_5$) and $BaSiO_3$, meanwhile, both seem to be stable up to relatively high temperatures.[53−55] The latter has even been shown to have catalytic properties.[56]

Cr−Si-System. As Cr_2O_3 occurs in as many as 7 (5) of the top 20 (10) transitions, it can be inferred to possess significant CLOU capabilities. Even though there are examples of chromium OCs,[6,57−60] this conclusion is still unexpected. In particular, such materials have not been as extensively studied as those based on Mn, Cu, or Fe, and, to the best of our knowledge, never for CLOU. At the same time, Cr_2O_3 is a well-known catalyst[61] and has been shown to be one of the dominant phases in bimetallic Cr−Fe and Cu−Cr OCs.[59] Our results should, therefore, be regarded as an indication that

https://doi.org/10.1021/acs.jpcc.2c08545
J. Phys. Chem. C 2023, 127, 9437−9451

further investigations of chromium oxides would be worthwhile.

Three of the transitions are almost identical but involve Na, K, and Rb, respectively,

$$\frac{2}{3}Cr_2O_3 + \frac{8}{3}K_2Si_2O_5 + O_2 \rightleftharpoons \frac{4}{3}K_2CrO_4 + \frac{4}{3}K_2Si_4O_9 \quad (11)$$

$$\frac{2}{3}Cr_2O_3 + \frac{10}{3}Rb_2Si_2O_5 + O_2 \rightleftharpoons \frac{4}{3}Rb_2CrO_4 + \frac{2}{3}Rb_6Si_{10}O_{23} \quad (12)$$

$$2Cr_2O_3 + \frac{8}{3}Na_2Si_2O_5 + O_2 \rightleftharpoons \frac{4}{3}Na_2CrO_4 + \frac{8}{3}NaCrSi_2O_6 \quad (13)$$

In fact, all lead to the formation of $(Na,K,Rb)_2CrO_4$. These phases have at the very least been experimentally characterized[62] and, in the case of $(Na,K)_2CrO_4$, observed to possess some catalytic ability.[63,64] This also applies to $(Na,K,Rb)_2Si_2O_5$,[65−67] which is found on the left-hand side of the equations. The composition of the second product, on the other hand, takes the form of $K_2Si_4O_9$, $Rb_6Si_{10}O_{23}$, and kosmochlor ($NaCrSi_2O_6$), respectively. Specifically, the former has been identified as a major phase in chemical looping gasification with potassium modified Mn-based OC[68] while both of the latter have been successfully synthesized and characterized.[69,70]

Additionally, two transitions based on K and Rb lead to the formation of $(K,Rb)_2CrO_4$ together with quartz (SiO_2),

$$\frac{2}{3}Cr_2O_3 + \frac{4}{3}K_2Si_4O_9 + O_2 \rightleftharpoons \frac{16}{3}SiO_2 + \frac{4}{3}K_2CrO_4 \quad (14)$$

$$\frac{2}{3}Cr_2O_3 + \frac{4}{9}Rb_6Si_{10}O_{23} + O_2 \rightleftharpoons \frac{40}{9}SiO_2 + \frac{4}{3}Rb_2CrO_4 \quad (15)$$

The two Ba-based transitions both lead to the formation of $BaCrO_4$ that, along with $SrCrO_4$, presumably has some photocatalytic properties,[71]

$$\frac{2}{3}Cr_2O_3 + \frac{8}{3}Ba_2Si_3O_8 + O_2 \rightleftharpoons \frac{4}{3}BaCrO_4 + 4BaSi_2O_5 \quad (16)$$

$$\frac{2}{3}Cr_2O_3 + 4BaSiO_3 + O_2 \rightleftharpoons \frac{4}{3}BaCrO_4 + \frac{4}{3}Ba_2Si_3O_8 \quad (17)$$

These also involve $BaSi_2O_5$ and $BaSiO_3$ as well as $Ba_2Si_3O_8$, the latter of which should be stable at even higher temperatures than the two former[53,72]

Mn−Si-System. As was mentioned in the previous section, manganese oxides are the most common candidates, and it is therefore not surprising that the top 20 (10) include no less than 8 (4). Intriguingly, 6 (4) involve Mn_7SiO_{12}, which is known to possess CLOU properties,[73] This can be seen as a direct confirmation that the approach employed in this study leads to reliable predictions. While there are few other similarities, two feature a synthetic variant of the mineral cordierite ($Mn_2Al_4Si_5O_{18}$), about which there exists very little information,[74]

$$\frac{7}{3}Mn_2Al_4Si_5O_{18} + O_2 \rightleftharpoons \frac{19}{3}SiO_2 + \frac{14}{3}Al_2SiO_5 + \frac{2}{3}Mn_7SiO_{12} \quad (18)$$

$$\frac{19}{3}Al_2O_3 + \frac{7}{3}Mn_2Al_4Si_5O_{18} + O_2 \rightleftharpoons Al_2SiO_5 + \frac{2}{3}Mn_7SiO_{12} \quad (19)$$

In both these cases, the product is a combination of Mn_7SiO_{12} and Al_2SiO_5. There is evidence that the latter should not only be stable at practically relevant temperatures[75] but might even have catalytic properties.[76]

There is also a pair of Ca-based candidates that both lead to the formation of the known catalyst $CaSiO_3$,[56]

$$\frac{7}{6}CaMn_4Si_5O_{15} + O_2 \rightleftharpoons 4SiO_2 + \frac{7}{6}CaSiO_3 + \frac{2}{3}Mn_7SiO_{12} \quad (20)$$

$$\frac{17}{6}Ca_2SiO_4 + \frac{1}{2}Mn_7SiO_{12} + O_2 \rightleftharpoons \frac{7}{6}Ca_2Mn_3O_8 + \frac{10}{3}CaSiO_3 \quad (21)$$

In the first of the two transitions, there is a single reduced phase in the form of the mineral rhodonite ($CaMn_4Si_5O_{15}$).[77] The second, meanwhile, involves Ca_2SiO_4 and $Ca_2Mn_3O_8$, which should both be stable within the temperature range of interest.[78−80] Interestingly, the former has been found to act as an OC[81] while the latter possesses catalytic abilities.[80]

Though Mg is found in several known OCs,[34,59] it only occurs in a single transition (17th) among the top 20,

$$\frac{14}{3}MgMnSiO_4 + O_2 \rightleftharpoons \frac{5}{3}SiO_2 + \frac{7}{3}Mg_2SiO_4 + \frac{2}{3}Mn_7SiO_{12} \quad (22)$$

Nevertheless, the reactant $MgMnSiO_4$ seems to have a relatively high stability since it can be synthesized via a solid state reaction at 1250 °C.[82] Mg_2SiO_4, on the other hand, can act as a catalyst,[83] but should not be expected to function as an OC in itself, unlike the second product Mn_7SiO_{12}.

Ba is involved in three transitions together with Mn and Si,

$$\frac{32}{3}BaSi_2O_5 + \frac{14}{3}Ba_2MnSi_2O_7 + O_2 \rightleftharpoons 10Ba_2Si_3O_8 + \frac{2}{3}Mn_7SiO_{12} \quad (23)$$

$$4Ba_2MnSi_2O_7 + O_2 \rightleftharpoons 2Mn_2O_3 + 8BaSiO_3 \quad (24)$$

$$2Ba_2SiO_4 + 2Ba_2MnSi_2O_7 + O_2 \rightleftharpoons 2BaMnO_3 + 6BaSiO_3 \quad (25)$$

Similarly to the cases discussed earlier, the first leads to the formation Mn_7SiO_{12} $Ba_2MnSi_2O_7$, which should be stable up to at least 1200 °C,[84] appear as a reactant in the other two candidates. In addition, both lead to the formation of $BaSiO_3$ together with the good OCs Mn_2O_3 and the perovskite $BaMnO_3$,[85] respectively.

Remaining Transitions. Interestingly, only the last two of the top 20 candidates are based on transition metals other than

https://doi.org/10.1021/acs.jpcc.2c08545
J. Phys. Chem. C 2023, 127, 9437−9451

Fe, Cr, or Mn. The first of these should be regarded as very promising,

$$4VO_2 + 2Sc_2Si_2O_7 + O_2 \rightleftharpoons 4SiO_2 + 4ScVO_4 \quad (26)$$

Specifically, VO_2 has been shown to function as an OC[86] while both $ScVO_4$ and $Sc_2Si_2O_7$ have a high-temperature stability,[87−89] By contrast, the second candidate is one of the few that involves a phase, $K_4CuSi_2O_7$, for which no record exists in the literature,

$$4K_4CuSi_2O_7 + O_2 \rightleftharpoons 4KCuO_2 + 4K_2SiO_3 + 2K_2Si_2O_5 \quad (27)$$

More information is available regarding $KCuO_2$, but it decomposes at temperatures higher than about 450 °C,[90] and K_2SiO_3, which seems to have some catalytic properties.[56] This case exemplifies the fact that we cannot guarantee that the proposed transitions will occur.

The Top 20 Candidates without Si. Since Si is found in each of the first 57 entries, we deem it worthwhile to also consider the list obtained when excluding this element. Interestingly, this means that a vast majority (14) of the top 20 candidates are instead based on Al.

Fe-Based without Si. The highest-ranking transition reveals the main weakness in our methodology,

$$4Fe_3O_4 + O_2 \rightleftharpoons 6Fe_2O_3 \quad (28)$$

More precisely, it involves Fe_3O_4/Fe_2O_3, which presumably does not possess any CLOU capability between 950 and 1000 °C despite being one of the best known and most extensively studied OCs.[34] The reason for this discrepancy is that we have chosen to use wide temperature and pressure intervals in the screening process to reduce the risk of overlooking interesting candidates. Inevitably, this leads to the inclusion of some that do not actually possess CLOU properties.

Since the thermodynamics could become more favorable in the presence of additional phases, it is noteworthy that Fe_3O_4, or Fe_2O_3, appears in five more of the top 20 candidates. Three of these also feature $RbFe_{11}O_{17}$, of which little is known except that it has a magnetoplumbite structure,[91]

$$4Fe_2CuO_4 + 4RbFe_{11}O_{17} + O_2 \rightleftharpoons 26Fe_2O_3 + 4RbCuO_2 \quad (29)$$

$$Mn_2O_3 + 2RbFe_{11}O_{17} + O_2 \rightleftharpoons 11Fe_2O_3 + 2RbMnO_3 \quad (30)$$

$$4Fe_3O_4 + \frac{12}{11}Rb_2TiO_3 + O_2 \rightleftharpoons \frac{12}{11}RbFe_{11}O_{17} + \frac{6}{11}Rb_2Ti_2O_5 \quad (31)$$

The two first cases are questionable, however, since Fe_2CuO_4 decomposes already at 500 °C[92] while there is no reference of $RbMnO_3$ in the literature. The third transition is more relevant since Rb_2TiO_3 and $Rb_2Ti_2O_5$ have both been experimentally characterized.[93,94]

There are also two Fe-based candidates that both involve a pair of perovskites,

$$4Fe_3O_4 + 12NdAlO_3 + O_2 \rightleftharpoons 6Al_2O_3 + 12NdFeO_3 \quad (32)$$

$$4Fe_3O_4 + 12LaAlO_3 + O_2 \rightleftharpoons 6Al_2O_3 + 12LaFeO_3 \quad (33)$$

This class of materials has received significant interest as OCs for a variety of CLC processes,[95] including CLOU.[32] Even though neither $(Nd,La)AlO_3$ nor $(Nd,La)FeO_3$ have been explored in this context, they have all been shown to possess catalytic properties as well as a high thermal stability.[96−99]

The first of the two final Fe-based transitions shows even more promise,

$$22Ca_2Fe_2O_5 + 2CaMn_2O_4 + O_2 \rightleftharpoons 22CaFe_2O_4 + 4Ca_6MnO_8 \quad (34)$$

In particular, it features three phases, specifically $Ca_2Fe_2O_5$, $CaMn_2O_4$, and $CaFe_2O_4$, that are known OCs.[100,101] There exists no information regarding Ca_6MnO_8, however.

The last case, which involves boron, is less interesting from a practical perspective because of the relative scarceness of this element,

$$2Fe_3BO_5 + O_2 \rightleftharpoons 2Fe_3BO_6 \quad (35)$$

In addition, the Fe_3BO_6 phase has never been reported, even though Fe_3BO_5 has been explored as a catalyst.[102]

Al−Mn-System. There are three additional Mn-based candidates, which all involve Al,

$$6MnAl_2O_4 + O_2 \rightleftharpoons 6Al_2O_3 + 2Mn_3O_4 \quad (36)$$

$$\frac{4}{3}LaAlO_3 + \frac{8}{3}MnAl_2O_4 + O_2 \rightleftharpoons \frac{10}{3}Al_2O_3 + \frac{4}{3}LaMn_2O_5 \quad (37)$$

$$2Mn_2O_3 + \frac{16}{3}SrAl_2O_4 + O_2 \rightleftharpoons \frac{8}{3}SrAl_4O_7 + \frac{4}{3}Sr_2Mn_3O_8 \quad (38)$$

Interestingly, they also include at least one phase that is known to have CLOU properties. This applies not only to the aforementioned Mn_2O_3/Mn_3O_4 pair but also $MnAl_2O_4$.[103] In addition, $SrAl_2O_4$, $SrAl_4O_7$, $LaMn_2O_5$, and $LaAlO_3$ have been shown to possess catalytic capabilities.[104,105] No record of $Sr_2Mn_3O_8$ could be found in the literature, however.

Al−Cr-System. A large number of transitions involve Cr (6), and most commonly Cr_2O_3 (5), together with Al. The first four candidates are very similar, since the catalysts Cr_2O_3 and $(Ba,Sr)CrO_4$ always appear on the reduced and oxidized side, respectively,

$$\frac{2}{3}Cr_2O_3 + \frac{4}{3}BaAl_4O_7 + O_2 \rightleftharpoons \frac{8}{3}Al_2O_3 + \frac{4}{3}BaCrO_4 \quad (39)$$

$$\frac{2}{3}Cr_2O_3 + \frac{4}{3}SrAl_4O_7 + O_2 \rightleftharpoons \frac{8}{3}Al_2O_3 + \frac{4}{3}SrCrO_4 \quad (40)$$

$$\frac{2}{3}Cr_2O_3 + \frac{8}{3}BaAl_2O_4 + O_2 \rightleftharpoons \frac{4}{3}BaAl_4O_7 + \frac{4}{3}BaCrO_4 \quad (41)$$

$$\frac{2}{3}Cr_2O_3 + \frac{8}{3}SrAl_2O_4 + O_2 \rightleftharpoons \frac{4}{3}SrAl_4O_7 + \frac{4}{3}SrCrO_4 \quad (42)$$

Moreover, $(Ba,Sr)Al_4O_7$ either appears as a product, in addition to $(Ba,Sr)Al_2O_4$, or a reactant, together with Al_2O_3. There is evidence to suggest that all of these phases are sufficiently stable,[106] In addition, $BaAl_2O_4$ has been shown to function as an OC,[44] and $SrAl_2O_4$ as a catalyst.

It is worth noting that the last two transitions, which involve Na and Ca, respectively, have much in common with those discussed above,

https://doi.org/10.1021/acs.jpcc.2c08545
J. Phys. Chem. C 2023, 127, 9437−9451

$$\frac{2}{3}Cr_2O_3 + \frac{8}{3}NaAlO_2 + O_2 \rightleftharpoons \frac{4}{3}Al_2O_3 + \frac{4}{3}Na_2CrO_4 \quad (43)$$

$$\frac{1}{3}Ca_3Al_4O_9 + \frac{2}{3}CaCr_2O_4 + O_2 \rightleftharpoons \frac{1}{3}CaAl_4O_7 + \frac{4}{3}CaCrO_4 \quad (44)$$

This is especially true for the latter since the $(Ba,Sr,Ca)Cr_2O_4$, $(Ba,Sr,Ca)Al_4O_7$, and $(Ba,Sr,Ca)CrO_4$ phases can be assumed to display similar properties. Only $CaCr_2O_4$ has been shown to form spontaneously during solid fuel combustion,[107] however. Even so, experiments indicate that $CaAl_4O_7$ and $CaCrO_4$ are also stable up to relatively high temperatures.[108,109] Unfortunately, there seems to be no information available regarding $Ca_3Al_4O_9$. The Na-based candidate is, nevertheless, more interesting because Na_2CrO_4 is catalytic while $NaAlO_2$ has been shown to enhance the performance of an Fe-based OC.[110]

Remaining Transitions without Si. Two of the final three candidates among the top 20 both involve Cu,

$$2BaAl_2O_4 + 4AlCuO_2 + O_2 \rightleftharpoons 4CuO + 2BaAl_4O_7 \quad (45)$$

$$4AlCuO_2 + 2SrAl_2O_4 + O_2 \rightleftharpoons 4CuO + 2SrAl_4O_7 \quad (46)$$

which should both be regarded as fairly promising since $(Ba,Sr)Al_2O_4$ are catalysts and CuO/CuO_2 is one the best-known OCs. Also, there is evidence to suggest that $(Ba,Sr)Al_4O_7$ as well as $AlCuO_2$ display good thermal stability.[111]

The last remaining transition is unlikely to be of practical relevance,

$$4KAlO_2 + Na_7Al_3O_8 + O_2 \rightleftharpoons 4KO + 7NaAlO_2 \quad (47)$$

First, KO has a strong tendency to react with water to form hydroxides[112] while little is known about $Na_7Al_3O_8$.[113] This is unfortunate since $KAlO_2$ possesses catalytic properties,[114] as well as a high thermal stability,[115] and $NaAlO_2$ has been used in CLC processes.

CONCLUSIONS

This paper is focused on a comprehensive study of candidate OCs for CLOU via a high-throughput screening method. The data were, more precisely, retrieved from the OQMD, in the form of ab initio calculations for all mono-, bi-, and trimetallic alloys and mixed oxides. We have more precisely used this information to construct convex hulls for all available ratios between the selected sets of elements with respect to the oxygen chemical potential. Identification of candidates was then achieved by plotting Ellingham diagrams and comparing the curves for each of the possible transitions with the requirement for CLOU. Accordingly, the transformation between the oxidized and reduced state should take place somewhere between 750 and 1050 °C under an oxygen partial pressure of 5 kPa. To account for the inherent uncertainty in the calculations, all transitions were included that crossed the aforementioned temperature interval between 10^{-6} MPa. This allowed us to identify 14030 potential OC materials out of a total of 260320 convex hulls. When only monometallic oxides were considered, however, the former number is reduced to just 20. This clearly shows that it is necessary to consider systems that involve at least two different metals to have a reasonable chance of discovering novel OCs.

The individual transitions were then ranked based on their average abundance. As expected, the top of the leaderboard is dominated by Si since it is one of the most abundant elements in the Earth's crust. Strong evidence for the efficacy of the methodology applied in this study is that manganese, copper, and iron, which are found in the best OCs, appear the most frequently in the entire list of candidates. Interestingly, chromium is just as common, even though materials based on this element have, to the best of our knowledge, never before been considered for this particular application. In fact, the most frequently appearing compounds among the highest ranking candidates are Cr_2O_3 and Mn_7SiO_{12}, which have been shown to possess catalytic and CLOU capabilities, respectively. Other elements that are deemed worthwhile to explore include Ba; K; Rb; Na; and V, especially if combined with Mn; Cu; Fe; or Cr. The same applies to Al and Si due to their high abundance, even though they are unlikely to confer CLOU properties given their relatively low occurrence among all candidates. The above conclusions appear even more robust if one also considers the number of possible OC materials that could be produced via chemical reactions with common ash elements. In particular, it can be concluded that materials based on Mn followed by Cu, Cr, and Fe have the highest probability of forming new OCs with CLOU properties through such interactions. Even so, it should be possible to use the data generated in this study to identify a material that is particularly suitable for a specific fuel.

Further analysis of the 20 highest-ranking candidates, with and without Si, reveals that most are not only stable in the temperature interval of interest but also possess catalytic capabilities. In a few cases these have even been used as OCs in the CLC processes, which is true for Mn_7SiO_{12}; $Ca_2Fe_2O_5$; $CaMn_2O_4$; $CaFe_2O_4$; $MnAl_2O_4$; and $BaAl_2O_4$ as well as Mn_2O_3/Mn_3O_4; CuO/CuO_2; and Fe_3O_4/Fe_2O_3. In addition, it is not uncommon that several transitions feature structurally similar phases in which one of the elements has been replaced by a neighbor in the periodic table. This is, for instance, observed for the alkali metals Na, K, and Rb as well as the alkaline earth metals Ba and Sr. Mixtures of these candidates should, moreover, result in new CLOU materials, which paves the way for the discovery of high-entropy stabilized OCs.

Note that a more exhaustive and detailed analysis is beyond the scope of this study. Additionally, it is questionable in terms of relevance due to the limitations in the information generated from the high-throughput screening. We have, for instance, not accounted for a number of key aspects that determine the usefulness of a given OC. This includes the chemical and mechanical robustness or, in other words, the tendency for fouling, attrition, and agglomeration. Indeed, such issues mean that many OCs with high OTCs and favorable thermodynamic properties cannot be used in CLC without support.[4,34] Hence, it is imperative that this exploratory effort is followed by more detailed experimental investigations of a selection of the most promising candidates.

As we have indicated, the number of potential materials can be significantly reduced through the application of chemical knowledge and comparisons with known OCs. Still, extensive possibilities exist to refine and extend the procedure outlined in this manuscript. According to our tests, a higher accuracy would, for example, be achieved by taking the temperature-dependent vibrational contribution to the free energy into

https://doi.org/10.1021/acs.jpcc.2c08545
J. Phys. Chem. C 2023, 127, 9437−9451

account (see Supplementary Note S2, Table S1, and Figure S1). In addition, it could be relevant to compare the results obtained when using data retrieved from different databases, such as the Materials Project database[22] and the aflowlib.org library.[23,24] While it is entirely feasible to consider systems with four metallic elements, or more, such efforts would probably be limited by a lack of first-principles data. Even so, we believe that our study clearly shows that the main obstacle to the discovery of novel OCs is the experimental efforts required to properly assess the viability of candidate materials identified via high-throughput screening.

■ ASSOCIATED CONTENT

Supporting Information

The Supporting Information is available free of charge at https://pubs.acs.org/doi/10.1021/acs.jpcc.2c08545.

Validation via comparison with experiments and phononic corrections; explanation of method for obtaining phase mixtures; formation of OCs through interaction with ash components; additional tables and figures (PDF)

List of unfiltered candidates (CSV)

List of filtered candidates (CSV)

■ AUTHOR INFORMATION

Corresponding Author

Anders Hellman − *Chalmers University of Technology,, Department of Physics, SE-412 96 Gothenburg, Sweden;* orcid.org/0000-0002-1821-159X; Email: anders.hellman@chalmers.se

Authors

Joakim Brorsson − *Chalmers University of Technology,, Department of Physics, SE-412 96 Gothenburg, Sweden;* orcid.org/0000-0002-7118-4930

Viktor Rehnberg − *Chalmers University of Technology,, Department of Physics, SE-412 96 Gothenburg, Sweden*

Adam A. Arvidsson − *Chalmers University of Technology,, Department of Physics, SE-412 96 Gothenburg, Sweden;* orcid.org/0000-0002-3107-8367

Henrik Leion − *Chalmers University of Technology,, Department of Chemistry and Chemical Engineering, SE-412 96 Gothenburg, Sweden;* orcid.org/0000-0002-9716-2553

Tobias Mattisson − *Chalmers University of Technology,, Department of Space, Earth and Environment, SE-412 96 Gothenburg, Sweden;* orcid.org/0000-0003-3942-7434

Complete contact information is available at: https://pubs.acs.org/10.1021/acs.jpcc.2c08545

Notes

The authors declare no competing financial interest.

■ ACKNOWLEDGMENTS

The authors express their gratitude to Ivana Staničić for many helpful discussions. This work was funded by the Swedish Research Council (2020-03487) and the computations were enabled by resources provided by the Swedish National Infrastructure for Computing (SNIC) at NSC and C3SE partially funded by the Swedish Research Council through grant agreement no. SNIC 2021/3-41, SNIC 2021/5-623, SNIC 2021/5-561, and SNIC 2022/5-156.

■ REFERENCES

(1) Lyngfelt, A.; Leckner, B.; Mattisson, T. A fluidized-bed combustion process with inherent CO2 separation; application of chemical-looping combustion. *Chem. Eng. Sci.* **2001**, *56*, 3101−3113.

(2) De Vos, Y.; Jacobs, M.; Van Der Voort, P.; Van Driessche, I.; Snijkers, F.; Verberckmoes, A. Development of Stable Oxygen Carrier Materials for Chemical Looping Processes—Review. *Catalysts* **2020**, *10*, 926.

(3) Qasim, M.; Ayoub, M.; Ghazali, N. A.; Aqsha, A.; Ameen, M. Recent Advances and Development of Various Oxygen Carriers for the Chemical Looping Combustion Process: A Review. *Ind. Eng. Chem. Res.* **2021**, *60*, 8621−8641.

(4) Alalwan, H. A.; Alminshid, A. H. CO2 capturing methods: Chemical looping combustion (CLC) as a promising technique. *Science of The Total Environment* **2021**, *788*, 147850.

(5) Wang, D.; Joshi, A.; Fan, L.-S. Chemical looping technology − a manifestation of a novel fluidization and fluid-particle system for CO2 capture and clean energy conversions. *Powder Technol.* **2022**, *409*, 117814.

(6) Zhu, X.; Imtiaz, Q.; Donat, F.; Müller, C. R.; Li, F. Chemical looping beyond combustion − a perspective. *Energy Environ. Sci.* **2020**, *13*, 772−804.

(7) Cheng, Z.; Qin, L.; Fan, J. A.; Fan, L.-S. New Insight into the Development of Oxygen Carrier Materials for Chemical Looping Systems. *Engineering* **2018**, *4*, 343−351.

(8) Staničić, I.; Hanning, M.; Deniz, R.; Mattisson, T.; Backman, R.; Leion, H. Interaction of oxygen carriers with common biomass ash components. *Fuel Process. Technol.* **2020**, *200*, 106313.

(9) Kwong, K.; Mao, R.; Scott, S.; Dennis, J.; Marek, E. Analysis of the rate of combustion of biomass char in a fluidised bed of CLOU particles. *Chemical Engineering Journal* **2021**, *417*, 127942.

(10) Mattisson, T.; Lyngfelt, A.; Leion, H. Chemical-looping with oxygen uncoupling for combustion of solid fuels. *International Journal of Greenhouse Gas Control* **2009**, *3*, 11−19.

(11) Azar, C.; Lindgren, K.; Obersteiner, M.; Riahi, K.; van Vuuren, D. P.; den Elzen, K. M. G. J.; Möllersten, K.; Larson, E. D. The feasibility of low CO_2 concentration targets and the role of bio-energy with carbon capture and storage (BECCS). *Climatic Change* **2010**, *100*, 195−202.

(12) Bui, M.; Adjiman, C. S.; Bardow, A.; Anthony, E. J.; Boston, A.; Brown, S.; Fennell, P. S.; Fuss, S.; Galindo, A.; Hackett, L. A.; et al. Carbon capture and storage (CCS): the way forward. *Energy Environ. Sci.* **2018**, *11*, 1062−1176.

(13) Gasser, T.; Guivarch, C.; Tachiiri, K.; Jones, C. D.; Ciais, P. Negative emissions physically needed to keep global warming below 2°C. *Nat. Commun.* **2015**, *6*, 7958.

(14) Abad, A.; Adánez-Rubio, I.; Gayán, P.; García-Labiano, F.; de Diego, L. F.; Adánez, J. Demonstration of chemical-looping with oxygen uncoupling (CLOU) process in a 1.5kWth continuously operating unit using a Cu-based oxygen-carrier. *International Journal of Greenhouse Gas Control* **2012**, *6*, 189−200.

(15) Adánez-Rubio, I.; Samprón, I.; Izquierdo, M. T.; Abad, A.; Gayán, P.; Adánez, J. Coal and biomass combustion with CO2 capture by CLOU process using a magnetic Fe-Mn-supported CuO oxygen carrier. *Fuel* **2022**, *314*, 122742.

(16) Peltola, P.; Saari, J.; Tynjälä, T.; Hyppänen, T. Process integration of chemical looping combustion with oxygen uncoupling in a biomass-fired combined heat and power plant. *Energy* **2020**, *210*, 118550.

(17) Lyngfelt, A.; Leckner, B. A 1000 MWth boiler for chemical-looping combustion of solid fuels − Discussion of design and costs. *Applied Energy* **2015**, *157*, 475−487.

(18) Mishra, A.; Li, F. Chemical looping at the nanoscale—challenges and opportunities. Current Opinion in Chemical Engineering. *Nanotechnology/Separation Engineering* **2018**, *20*, 143−150.

(19) Lau, C. Y.; Dunstan, M. T.; Hu, W.; Grey, C. P.; Scott, S. A. Large scale in silico screening of materials for carbon capture through chemical looping. *Energy Environ. Sci.* **2017**, *10*, 818−831.

(20) Saal, J. E.; Kirklin, S.; Aykol, M.; Meredig, B.; Wolverton, C. Materials Design and Discovery with High-Throughput Density Functional Theory: The Open Quantum Materials Database (OQMD). *JOM* **2013**, *65*, 1501−1509.
(21) Kirklin, S.; Saal, J. E.; Meredig, B.; Thompson, A.; Doak, J. W.; Aykol, M.; Rühl, S.; Wolverton, C. The Open Quantum Materials Database (OQMD): assessing the accuracy of DFT formation energies. *npj Comput. Mater.* **2015**, *1*, 1−15.
(22) Jain, A.; Ong, S. P.; Hautier, G.; Chen, W.; Richards, W. D.; Dacek, S.; Cholia, S.; Gunter, D.; Skinner, D.; Ceder, G.; et al. Commentary: The Materials Project: A materials genome approach to accelerating materials innovation. *APL Materials* **2013**, *1*, 011002.
(23) Curtarolo, S.; Setyawan, W.; Hart, G. L.; Jahnatek, M.; Chepulskii, R. V.; Taylor, R. H.; Wang, S.; Xue, J.; Yang, K.; Levy, O.; et al. AFLOW: An automatic framework for high-throughput materials discovery. *Comput. Mater. Sci.* **2012**, *58*, 218−226.
(24) Curtarolo, S.; Setyawan, W.; Wang, S.; Xue, J.; Yang, K.; Taylor, R. H.; Nelson, L. J.; Hart, G. L.; Sanvito, S.; Buongiorno-Nardelli, M.; et al. AFLOWLIB.ORG: A distributed materials properties repository from high-throughput ab initio calculations. *Comput. Mater. Sci.* **2012**, *58*, 227−235.
(25) Draxl, C.; Scheffler, M. The NOMAD laboratory: from data sharing to artificial intelligence. *Journal of Physics: Materials* **2019**, *2*, 036001.
(26) The Open Quantum Materials Database. accessed 2022−01−16; http://oqmd.org/.
(27) Blöchl, P. E. Projector augmented-wave method. *Phys. Rev. B* **1994**, *50*, 17953−17979.
(28) Kresse, G.; Joubert, D. From ultrasoft pseudopotentials to the projector augmented-wave method. *Phys. Rev. B* **1999**, *59*, 1758−1775.
(29) Kresse, G.; Furthmüller, J. Efficient iterative schemes for ab initio total-energy calculations using a plane-wave basis set. *Phys. Rev. B* **1996**, *54*, 11169.
(30) Perdew, J. P.; Burke, K.; Ernzerhof, M. Generalized Gradient Approximation Made Simple. *Phys. Rev. Lett.* **1996**, *77*, 3865−3868.
(31) Mattisson, T. Materials for Chemical-Looping with Oxygen Uncoupling. *ISRN Chemical Engineering* **2013**, *2013*, 526375.
(32) Mishra, A.; Li, T.; Li, F.; Santiso, E. E. Oxygen Vacancy Creation Energy in Mn-Containing Perovskites: An Effective Indicator for Chemical Looping with Oxygen Uncoupling. *Chem. Mater.* **2019**, *31*, 689−698.
(33) Wang, M.; Zhang, S.; Xia, M.; Wang, M. A Theoretical Study of the Oxygen Release Mechanisms of a Cu-Based Oxygen Carrier during Chemical Looping with Oxygen Uncoupling. *Catalysts* **2022**, *12*, 332−332.
(34) Imtiaz, Q.; Hosseini, D.; Müller, C. R. Review of Oxygen Carriers for Chemical Looping with Oxygen Uncoupling (CLOU): Thermodynamics, Material Development, and Synthesis. *Energy Technology* **2013**, *1*, 633−647.
(35) Rydén, M.; Leion, H.; Mattisson, T.; Lyngfelt, A. Combined oxides as oxygen-carrier material for chemical-looping with oxygen uncoupling. *Applied Energy* **2014**, *113*, 1924−1932.
(36) Zeng, L.; Cheng, Z.; Fan, J. A.; Fan, L.-S.; Gong, J. Metal oxide redox chemistry for chemical looping processes. *Nature Reviews Chemistry* **2018**, *2*, 349−364.
(37) Lee, D. D.; Choy, J. H.; Lee, J. K. Computer generation of binary and ternary phase diagrams via a convex hull method. *J. Phase Equilib.* **1992**, *13*, 365−372.
(38) Ong, S. P.; Wang, L.; Kang, B.; Ceder, G. Li-Fe-P-O2 Phase Diagram from First Principles Calculations. *Chem. Mater.* **2008**, *20*, 1798−1807.
(39) Ong, S. P.; Jain, A.; Hautier, G.; Kang, B.; Ceder, G. Thermal stabilities of delithiated olivine MPO_4 (M = Fe, Mn) cathodes investigated using first principles calculations. *Electrochem. Commun.* **2010**, *12*, 427−430.
(40) Dunstan, M. T.; Jain, A.; Liu, W.; Ong, S. P.; Liu, T.; Lee, J.; Persson, K. A.; Scott, S. A.; Dennis, J. S.; Grey, C. P. Large scale computational screening and experimental discovery of novel materials for high temperature CO2 capture. *Energy Environ. Sci.* **2016**, *9*, 1346−1360.
(41) Linstrom, P. J.; Mallard, W. G. The NIST Chemistry WebBook: A Chemical Data Resource on the Internet. *Journal of Chemical & Engineering Data* **2001**, *46*, 1059−1063.
(42) Reuter, K.; Scheffler, M. Composition, structure, and stability of RuO2(110) as a function of oxygen pressure. *Phys. Rev. B* **2001**, *65*, 65.
(43) Brunning, A. *Periodic Table of Element Hazard Symbols*; Andy Brunning/Compound Interest, 2019; https://www.compoundchem.com/2019advent/day15/.
(44) Wang, H.; Liu, G.; Veksha, A.; Dou, X.; Giannis, A.; Lim, T. T.; Lisak, G. Iron ore modified with alkaline earth metals for the chemical looping combustion of municipal solid waste derived syngas. *Journal of Cleaner Production* **2021**, *282*, 124467.
(45) Staničić, I.; Brorsson, J.; Hellman, A., Mattisson, T., Backman, R. Thermodynamic Analysis on the Fate of Ash Elements in Chemical Looping Combustion of Solid Fuels-Iron-Based Oxygen Carriers. *Energy Fuels* **2022**,.369648
(46) Vesborg, P. C. K.; Jaramillo, T. F. Addressing the terawatt challenge: scalability in the supply of chemical elements for renewable energy. *RSC Adv.* **2012**, *2*, 7933−7947.
(47) Albedwawi, S. H.; AlJaberi, A.; Haidemenopoulos, G. N.; Polychronopoulou, K. High entropy oxides-exploring a paradigm of promising catalysts: A review. *Materials & Design* **2021**, *202*, 109534.
(48) Schaller, W. T. Gillespite, a new mineral. *Journal of the Washington Academy of Sciences* **1922**, *12*, 7−8.
(49) Bloise, A. Synthesis and characterization of gillespite. *Appl. Phys. A: Mater. Sci. Process.* **2018**, *124*, 330.
(50) Ferreira, T.; Morrison, G.; Chance, W. M.; Calder, S.; Smith, M. D.; zur Loye, H.-C. $BaFe_4O_7$ and $K_{0.22}Ba_{0.89}Fe_4O_7$: Canted Antiferromagnetic Diferrites with Exceptionally High Magnetic Ordering Temperatures. *Chem. Mater.* **2017**, *29*, 2689−2693.
(51) Yu, H.-H.; Xue, X.-X.; Huang, D.-W. Crystallization on BaO-Fe_2O_3-SiO_2 glass-ceramic made from iron ore tailing. *Zhongguo Youse Jinshu Xuebao/Chinese Journal of Nonferrous Metals* **2008**, *18*, 2076−2081.
(52) Jang, T.-H.; Do, S.-H.; Lee, M.; Wu, H.; Brown, C. M.; Christianson, A. D.; Cheong, S.-W.; Park, J.-H. Physical properties of the quasi-two-dimensional square lattice antiferromagnet $Ba_2FeSi_2O_7$. *Phys. Rev. B* **2021**, *104*, 214434.
(53) Huntelaar, M.; Cordfunke, E. The ternary system $BaSiO_3$-$SrSiO_3$-SiO_3. *J. Nucl. Mater.* **1993**, *201*, 250−253.
(54) Gorelova, L. A.; Bubnova, R. S.; Krivovichev, S. V.; Krzhizhanovskaya, M. G.; Filatov, S. K. Thermal expansion and structural complexity of Ba silicates with tetrahedrally coordinated Si atoms. *J. Solid State Chem.* **2016**, *235*, 76−84.
(55) Gomes, E. O.; Moulton, B. J.; Cunha, T. R.; Gracia, L.; Pizani, P. S.; Andrés, J. Identifying and explaining vibrational modes of sanbornite (low-$BaSi_2O_5$) and $Ba_5Si_8O_{21}$: A joint experimental and theoretical study. *Spectrochimica Acta Part A: Molecular and Biomolecular Spectroscopy* **2021**, *248*, 119130.
(56) Sheikh, S.; Fazlinia, A. Preparation of Pyrido[2,3-b]indole Derivatives Using Silicates of Group 1 and 2 Metals. *Journal of Heterocyclic Chemistry* **2018**, *55*, 2291−2296.
(57) Dey, S.; Kumar, V. P. Supported and un-supported zinc and chromium oxide catalysts for lower temperature CO oxidation: A review. *Environmental Challenges* **2021**, *3*, 100061.
(58) Das, S.; Biswas, A.; Ghoroi, C.; Konar, B.; Paliwal, M. Oxidation of Ferrochrome Slag Using CO_2: A Possible O_2 Carrier in CLC Process. *Journal of Sustainable Metallurgy* **2022**, *8*, 343−359.
(59) Hashimi, H. A.; Chaalal, O. Correlating electronegativity in bimetallic oxygen carriers for chemical looping combustion. *Thermal Science and Engineering Progress* **2022**, *27*, 101170.
(60) Di, Z.; Yilmaz, D.; Biswas, A.; Cheng, F.; Leion, H. Spinel ferrite-contained industrial materials as oxygen carriers in chemical looping combustion. *Applied Energy* **2022**, *307*, 118298.
(61) Medasani, B. K.; Sushko, M. L.; Rosso, K. M.; Schreiber, D. K.; Bruemmer, S. M. Temperature Dependence of Self-Diffusion in

Cr_2O_3 from First Principles. *J. Phys. Chem. C* **2019**, *123*, 22139−22150.
(62) O'Hare, P.; Johnson, G. Rubidium chromate: standard molar enthalpies of solution and formation and the standard molar entropy at 298.15 K, enthalpy increments relative to 298.15 K, the high-temperature heat capacity, and temperatures, enthalpies, and entropies of transition and melting thermodynamic properties of Rb_2CrO_4 from 298.15 to 1500 K. *J. Chem. Thermodyn.* **1985**, *17*, 391−400.
(63) Wang, X.-M.; Zeng, Y.-N.; Jiang, L.-Q.; Wang, Y.-T.; Li, J.-G.; Kang, L.-L.; Ji, R.; Gao, D.; Wang, F.-P.; Yu, Q.; Wang, Y.-J.; Ji, A.-M.; Fang, Z. Highly stable $NaFeO_2$-Fe_3O_4 composite catalyst from blast furnace dust for efficient production of biodiesel at low temperature. *Industrial Crops and Products* **2022**, *182*, 114937.
(64) Li, Y.; Li, L.; Luo, S.; Huang, X.; Shen, J.; Jiang, C.; Jing, F. The role of K in tuning oxidative dehydrogenation of ethane with CO_2 to be selective toward ethylene. *Advanced Composites and Hybrid Materials* **2021**, *4*, 793−805.
(65) Yaakob, Z.; Padikkaparambil, S.; Binitha, N.; Resmi, R.; Suraja, V. Transesterification of ethylacetate over $Na_2Si_2O_5$ solid catalyst. *Chemical Engineering Transactions* **2011**, *24*, 103−108.
(66) Su, C.; McGinn, P. J. The effect of Ca^{2+} and Al^{3+} additions on the stability of potassium disilicate glass as a soot oxidation catalyst. *Applied Catalysis B: Environmental* **2013**, *138*−*139*, 70−78.
(67) de Jong, B.; Slaats, P.; Supèr, H.; Veldman, N.; Spek, A. Extended structures in crystalline phyllosilicates: silica ring systems in lithium, rubidium, cesium, and cesium/lithium phyllosilicate. *J. Non-Cryst. Solids* **1994**, *176*, 164−171.
(68) Liu, X.; Ma, J.; Hong, Q.; Ma, S.; Ge, H.; Song, T. In-situ catalytic effect of potassium on petroleum coke gasification with a Mn ore-based oxygen carrier. *Fuel* **2021**, *306*, 121763.
(69) Lapshin, A. E.; Borisova, N. B.; Ushakov, V. M.; Shepelev, Y. F. Structure and some thermodynamic characteristics of the polymorphs of rubidium silicate $Rb_6Si_{10}O_{23}$. *Russ. J. Inorg. Chem.* **2006**, *51*, 438−444.
(70) Posner, E. S.; Dera, P.; Downs, R. T.; Lazarz, J. D.; Irmen, P. High-pressure single-crystal X-ray diffraction study of jadeite and kosmochlor. *Physics and Chemistry of Minerals* **2014**, *41*, 695−707.
(71) Yin, J.; Zou, Z.; Ye, J. Photophysical and photocatalytic properties of new photocatalysts $MCrO_4$ (M = Sr, Ba). *Chem. Phys. Lett.* **2003**, *378*, 24−28.
(72) Takahashi, Y.; Masai, H.; Osada, M.; Ihara, R.; Fujiwara, T. Formation of spherulite and metastable phase in stoichiometric $Ba_2Si_3O_8$ glass. *Journal of the Ceramic Society of Japan* **2010**, *118*, 955−958.
(73) Jing, D.; Arjmand, M.; Mattisson, T.; Rydén, M.; Snijkers, F.; Leion, H.; Lyngfelt, A. Examination of oxygen uncoupling behaviour and reactivity towards methane for manganese silicate oxygen carriers in chemical-looping combustion. *International Journal of Greenhouse Gas Control* **2014**, *29*, 70−81.
(74) Knorr, K.; Meschke, M.; Winkler, B. Structural and magnetic properties of Co2Al4Si5O18 and Mn2Al4Si5O18 cordierite. *Physics and Chemistry of Minerals* **1999**, *26*, 521−529.
(75) Benisek, A.; Dachs, E. The accuracy of standard enthalpies and entropies for phases of petrological interest derived from density-functional calculations. *Contributions to Mineralogy and Petrology* **2018**, *173*, 90.
(76) Wang, Q.; Liang, C.; Zheng, Y.; Ashburn, N.; Oh, Y. J.; Kong, F.; Zhang, C.; Nie, Y.; Sun, J.; He, K.; et al. First principles study of the Mn-doping effect on the physical and chemical properties of mullite-family Al_2SiO_5. *Phys. Chem. Chem. Phys.* **2017**, *19*, 24991−25001.
(77) Shchipalkina, N. V.; Pekov, I. V.; Chukanov, N. V.; Zubkova, N. V.; Belakovskiy, D. I.; Britvin, S. N.; Koshlyakova, N. N. Vittinkiite, $MnMn_4[Si_5O_{15}]$, a member of the rhodonite group with a long history: definition as a mineral species. *Mineralogical Magazine* **2020**, *84*, 869−880.
(78) Mazarío-Fernández, A.; Torres-Pardo, A.; Varela, A.; Parras, M.; Martínez, J. L.; Fernández-Díaz, M. T.; Hernando, M.; González-Calbet, J. M. Atomically Resolved Short-Range Order at the Nanoscale in the Ca-Mn-O System. *Inorg. Chem.* **2017**, *56*, 11753−11761.
(79) Yao, Z.; Ma, X.; Lyu, S. Phase equilibria of the Al_2O_3−CaO−SiO_2-(0%, 5%, 10%) MgO slag system for non-metallic inclusions control. *Calphad* **2021**, *72*, 102227.
(80) Bihanic, C.; Diliberto, S.; Pelissier, F.; Petit, E.; Boulanger, C.; Grison, C. Eco-$CaMnO_x$: A Greener Generation of Eco-catalysts for Eco-friendly Oxidation Processes. ACS Sustainable. *Chem. Eng.* **2020**, *8*, 4044−4057.
(81) Jiang, H.; Li, C.; Chen, L.; Yan, S.; Lin, Y.; Zhao, Z.; Huang, Z.; Wang, S.; Huang, H.; Li, H. Dechlorination Performance of Chemical Looping Conversion Using Red Mud as an Oxygen Carrier. *Energy Fuels* **2022**, *36*, 9616−9627.
(82) Yamazaki, S.; Toraya, H. X-ray powder data for $MgMnSiO_4$ and $Mg_{0.6}Mn_{1.4}SiO_4$. *Powder Diffraction* **2001**, *16*, 115−119.
(83) Zhu, Q.; Wang, B.; Tan, T. Conversion of Ethanol and Acetaldehyde to Butadiene over MgO-SiO2 Catalysts: Effect of Reaction Parameters and Interaction between MgO and SiO_2 on Catalytic Performance. *ACS Sustainable Chem. Eng.* **2017**, *5*, 722−733.
(84) Sale, M.; Xia, Q.; Avdeev, M.; Ling, C. D. Crystal and Magnetic Structures of Melilite-Type $Ba_2MnSi_2O_7$. *Inorg. Chem.* **2019**, *58*, 4164−4172.
(85) Cao, D.; Luo, C.; Xing, W.; Cai, G.; Luo, T.; Wu, F.; Li, X.; Zhang, L. Coal-direct chemical looping hydrogen generation with $BaMnO_3$ perovskite oxygen carrier. *Fuel Process. Technol.* **2022**, *233*, 107296.
(86) Cao, J.; Ma, S.; Song, T. V_2O_5/TiO_2 acting as both oxygen carrier and catalyst for chemical looping oxidation of H_2S at a low temperature. *Fuel* **2022**, *320*, 123999.
(87) Dorogova, M.; Navrotsky, A.; Boatner, L. Enthalpies of formation of rare earth orthovanadates, $REVO_4$. *J. Solid State Chem.* **2007**, *180*, 847−851.
(88) Denisova, L. T.; Kargin, Y. F.; Chumilina, L. G.; Denisov, V. M. Heat capacity of $ScVO_4$ from 328 to 1000 K. *Inorg. Mater.* **2015**, *51*, 163−166.
(89) Ridley, M.; Opila, E. Variable thermochemical stability of $RE_2Si_2O_7$ (RE = Sc, Nd, Er, Yb, or Lu) in high-temperature high-velocity steam. *J. Am. Ceram. Soc.* **2022**, *105*, 1330−1342.
(90) Costa, G. A.; Kaiser, E. Structural and thermal properties of the alkaline cuprate $KCuO_2$. *Thermochim. Acta* **1995**, *269*−*270*, 591−598. Recent Advances in Thermal Analysis and Calorimetry.
(91) Galasso, F. S. In *Structure and Properties of Inorganic*; Galasso, F. S., Ed.; International Series of Monographs in Solid State Physics; Pergamon, 1970; pp 211−234.
(92) El-Shobaky, H.; Fahmy, Y. Cordierite as catalyst support for nanocrystalline CuO/Fe_2O_3 system. *Mater. Res. Bull.* **2006**, *41*, 1701−1713.
(93) Weiß, C.; Hoppe, R. What does solid state mean? New molecular aspects on the example of $Rb_2[TiO_3]$ [1], [2]. *Zeitschrift für anorganische und allgemeine Chemie* **1996**, *622*, 1019−1026.
(94) Federicci, R.; Baptiste, B.; Finocchi, F.; Popa, F.; Brohan, L.; Béneut, K.; Giura, P.; Rousse, G.; Descamps-Mandine, A.; Douillard, T.; Shukla, A.; Leridon, B. The crystal structure of $Rb_2Ti_2O_5$. *Acta Crystallographica Section B* **2017**, *73*, 1142−1150.
(95) Wang, X.; Gao, Y.; Krzystowczyk, E.; Iftikhar, S.; Dou, J.; Cai, R.; Wang, H.; Ruan, C.; Ye, S.; Li, F. High-throughput oxygen chemical potential engineering of perovskite oxides for chemical looping applications. *Energy Environ. Sci.* **2022**, *15*, 1512−1528.
(96) Muñoz, H. J.; Korili, S. A.; Gil, A. Progress and Recent Strategies in the Synthesis and Catalytic Applications of Perovskites Based on Lanthanum and Aluminum. *Materials* **2022**, *15*, 3288.
(97) Li, J.; Wei, M.; Li, L.; Tang, S. Citrate precursor synthesis of perovskite-type $NdAlO_3$ as a microwave dielectric material. *Journal of Materials Science: Materials in Electronics* **2020**, *31*, 15352−15360.
(98) Dionicio-Navarrete, M.; Arrieta-Gonzalez, C. D.; Quinto-Hernandez, A.; Casales-Diaz, M.; Zuñiga-Diaz, J.; Porcayo-Calderon, J.; Martinez-Gomez, L. Synthesis of $NdAlO_3$ Nanoparticles and

https://doi.org/10.1021/acs.jpcc.2c08545
J. Phys. Chem. C 2023, 127, 9437−9451

Evaluation of the Catalytic Capacity for Biodiesel Synthesis. *Nanomaterials* **2019**, *9*, 1545.
(99) Ciambelli, P.; Cimino, S.; De Rossi, S.; Lisi, L.; Minelli, G.; Porta, P.; Russo, G. $AFeO_3$ (A = La, Nd, Sm) and $LaFe_{1-x}Mg_xO_3$ perovskites as methane combustion and CO oxidation catalysts: structural, redox and catalytic properties. *Applied Catalysis B: Environmental* **2001**, *29*, 239−250.
(100) Wu, J.; Bai, L.; Tian, H.; Riley, J.; Siriwardane, R.; Wang, Z.; He, T.; Li, J.; Zhang, J.; Wu, J. Chemical looping gasification of lignin with bimetallic oxygen carriers. *International Journal of Greenhouse Gas Control* **2020**, *93*, 102897.
(101) Yan, B.; Liu, Z.; Wang, J.; Ge, Y.; Tao, J.; Cheng, Z.; Chen, G. Mn-doped $Ca_2Fe_2O_5$ oxygen carrier for chemical looping gasification of biogas residue: Effect of oxygen uncoupling. *Chemical Engineering Journal* **2022**, *446*, 137086.
(102) Cherkezova-Zheleva, Z.; Tsoncheva, T.; Tyuliev, G.; Mitov, I. Study of mixed valence iron borate catalysts in ethyl acetate oxidation process. *Applied Catalysis A: General* **2006**, *298*, 24−31.
(103) Miller, D. D.; Smith, M.; Shekhawat, D. Interaction of manganese with aluminosilicate support during high temperature (1100°C) chemical looping combustion of the Fe-Mn-based oxygen carrier. *Fuel* **2020**, *263*, 116738.
(104) Baidya, T.; van Vegten, N.; Verel, R.; Jiang, Y.; Yulikov, M.; Kohn, T.; Jeschke, G.; Baiker, A. SrO ·Al_2O_3 mixed oxides: A promising class of catalysts for oxidative coupling of methane. *J. Catal.* **2011**, *281*, 241−253.
(105) Feng, X.; Liu, R.; Zhang, S.; He, J.; Xu, X.; Xu, J.; Fang, X.; Wang, X. Study on the Structure-Reactivity Relationship of $LnMn_2O_5$ (Ln = La, Pr, Sm, Y) Mullite Catalysts for Soot Combustion. *Chemistry Africa* **2020**, *3*, 695−701.
(106) Allix, M.; Alahrache, S.; Fayon, F.; Suchomel, M.; Porcher, F.; Cardinal, T.; Matzen, G. Highly Transparent $BaAl_4O_7$ Polycrystalline Ceramic Obtained by Full Crystallization from Glass. *Adv. Mater.* **2012**, *24*, 5570−5575.
(107) Gong, H.; Huang, Y.; Hu, H.; Shi, M.; Fu, B.; Luo, C.; Yan, D.; Yao, H. The potential oxidation characteristics of $CaCr_2O_4$ during coal combustion with solid waste in a fluidized bed boiler: A thermogravimetric analysis. *Chemosphere* **2021**, *263*, 127974.
(108) Altay, A.; Carter, C.; Arslan, I.; Gülgün, M. Crystallization of $CaAl_4O_7$ and $CaAl_{12}O_{19}$ powders. *Philos. Mag.* **2009**, *89*, 605−621.
(109) Wu, Y.; Song, S.; Xv, Y.; Xue, Z. The formation mechanism and thermal stability of $CaCrO_4$. *IOP Conference Series: Earth and Environmental Science* **2020**, *514*, 052024.
(110) Li, J.; Zhang, X.; Li, X.; Wu, J.; Ma, J.; Guo, Q.; Liu, X. Research of coal−direct chemical looping hydrogen generation with iron−based oxygen carrier modified by $NaAlO_2$. *Canadian Journal of Chemical Engineering* **2021**, *99*, 578−589.
(111) Mahmood, K.; Abbasi, S.; Zahra, R.; Rehman, U. Investigation of large Seebeck effect by charge mobility engineering in $CuAlO_2$ thin films grown on Si substrate by thermal evaporation. *Ceram. Int.* **2018**, *44*, 17905−17908.
(112) Johnson, D., Ed. *Metals and Chemical Change*; The Royal Society of Chemistry, 2002; Chapter 25, pp 160−169.
(113) Barker, M. G.; Gadd, P. G.; Begley, M. J. Identification and characterisation of three novel compounds in the sodium−aluminium−oxygen system. *J. Chem. Soc., Dalton Trans.* **1984**, 1139−1146.
(114) Wei, Q.; Hu, J.; Zhang, H.; Wang, G.; Yang, X. Efficient Synthesis of Dimethyl Carbonate via Transesterification from Ethylene Carbonate with Methanol Using $KAlO_2/\gamma$−Al_2O_3 Heterogeneous Catalys. *ChemistrySelect* **2020**, *5*, 7826−7834.
(115) Kim, D. − G.; Moosavi-Khoonsari, E.; Jung, I. − H. Thermodynamic modeling of the K_2O−Al_2O_3 and K_2O−MgO−Al_2O_3 systems with emphasis on β− and β"−aluminas. *Journal of the European Ceramic Society* **2018**, *38*, 3188−3200.

https://doi.org/10.1021/acs.jpcc.2c08545
J. Phys. Chem. C 2023, 127, 9437−9451